Mode-coupling theory for the glassy dynamics of a diatomic probe molecule immersed in a simple liquid

S.-H. Chong, W. Götze, and A. P. Singh*
Physik-Department, Technische Universität München, 85747 Garching, Germany
(Received 23 August 2000; published 21 December 2000)

Generalizing the mode-coupling theory for ideal liquid-glass transitions, equations of motion are derived for the correlation functions describing the glassy dynamics of a diatomic probe molecule immersed in a simple glass-forming system. The molecule is described in the interaction-site representation and the equations are solved for a dumbbell molecule consisting of two fused hard spheres in a hard-sphere system. The results for the molecule's arrested position in the glass state and the reorientational correlators for angular-momentum index $\ell=1$ and $\ell=2$ near the glass transition are compared with those obtained previously within a theory based on a tensor-density description of the molecule in order to demonstrate that the two approaches yield equivalent results. For strongly hindered reorientational motion, the dipole-relaxation spectra for the α process can be mapped on the dielectric-loss spectra of glycerol if a rescaling is performed according to a suggestion by Dixon *et al.* [Phys. Rev. Lett. **65**, 1108 (1990)]. It is demonstrated that the glassy dynamics is independent of the molecule's inertia parameters.

DOI: 10.1103/PhysRevE.63.011206 PACS number(s): 61.20.Lc, 64.70.Pf, 61.25.Em

I. INTRODUCTION

The mode-coupling theory (MCT) for the evolution of structural relaxation in glass-forming liquids was originally developed for atomic systems and for mixtures of atoms or ions. Detailed tests of the theory have been provided through comparisons of the predictions for the hard-sphere system (HSS) with dynamic-light-scattering data for hard-sphere colloids, as can be inferred from Ref. [1] and the papers quoted therein. Quantitative tests have also been made by comparing molecular-dynamics-simulation data for a binary mixture with the MCT results for the model [2–4]. A series of general implications of the MCT equations were derived, such as scaling laws and relations between anomalous exponents describing power-law spectra and relaxation-time scales, which establish some universal features of the dynamics [5]. It was conjectured that these results also apply to molecular liquids. Indeed, there is a large body of literature, which is reviewed in Ref. [6], dealing with the analysis of data from experiments or from molecular-dynamics simulations for complicated systems in terms of the universal MCT formulas. These studies suggest that MCT describes some essential features of the glassy dynamics for molecular liquids. Therefore, it seems desirable to develop a detailed microscopic theory also for systems of nonspherical constituents.

A mode-coupling theory for molecular systems was studied in Refs. [7–12], where the structure is described by tensor-density fluctuations. The basic concepts of the MCT for simple systems such as density correlators and relaxation kernels have been generalized to infinite matrices. The equations for the nonergodicity parameters and critical amplitudes were solved. These quantities generalize the Debye-Waller factors of the arrested glass structure and characterize its changes with temperature. Comparison of the theoretical findings with molecular-dynamics-simulation data for water [9,11] and for a system of linear molecules [10] demonstrates that the theory can cope with microscopic details. However, the derived equations are so involved that further simplifications would be required before correlators or spectra could actually be calculated.

The simplest question of glassy dynamics of the rotational degrees of freedom concerns the motion of a single linear molecule in a simple liquid. This problem is equivalent to the study of a dilute solution of linear molecules in an atomic liquid as solvent. For this system, a MCT has been developed, generalizing the equation for a tagged particle in a simple liquid to an infinite-matrix equation for a tagged molecule [13]. The equations were solved for a molecule consisting of two fused hard spheres immersed in a HSS [13,14]. The validity of the universal laws for the reorientational dynamics was demonstrated. Characteristic differences for the α process between the relaxation for angular-momentum index $\ell=1$ and $\ell=2$ were identified which explain the differences between spectra measured for $\ell=1$ by dielectric-loss spectroscopy and for $\ell=2$ by depolarized-light-scattering spectroscopy. The experimentally established large ratio of the α relaxation times for the $\ell=2$-reorientational process and the longitudinal elastic modulus was also obtained [14]. These examples show that MCT can provide general insight into the glassy dynamics of rotational degrees of freedom that goes beyond the contents of the universal formulas.

Within the basic version of MCT, the tagged-particle-density-fluctuation correlator for wave number q considered as a function of time t, $\phi_q^s(t)$, or the dynamical structure factor for frequency ω, $S_q(\omega)$, can be written as $\phi_q^s(t)=\phi_q^{s*}(t/t_0)$ and $S_q(\omega)=S_q^*(\omega t_0)$. Here the functions $\phi_q^{s*}(\tilde{t})$ and $S_q^*(\tilde{\omega})$ are completely determined by the equilibrium structure. This holds for times outside the transient

*Present address: Mckinsey & Company, Inc., 80538 München, Germany.

regime, $t/t_0 \gg 1$, or for frequencies below the band of microscopic excitations, $\omega t_0 \ll 1$. The subtleties of the transient dynamics, like the dependence of oscillation frequencies on mass ratios, enter into the long-time dynamics and the low-frequency spectra via a common time scale t_0 only. This means that the statistical information on the long-time dynamics is determined up to a scale t_0 by the statistics of the system's orbits in configuration space rather than by the orbits in phase space. The glassy dynamics as described by functions like $\phi_q^s(t)$ or $S_q(\omega)$ deals with the probabilities of paths through the high-dimensional potential-energy landscape. The complicated dynamics on microscopic time scales is irrelevant in the long-time regime; it merely determines the scale t_0 for the exploration of the configuration space. The cited results of the MCT for simple systems and mixtures [5,15,16] are not valid for the mentioned theories for molecular systems [7–11,13,14], which imply isotope effects for the glassy dynamics. A change of the mass ratio of the molecule's constituents shifts the center of gravity, and the mode-coupling coefficients are thereby altered. This leads to shifts of the glass-transition temperature, the particle's localization lengths, and the like. In this respect a system of *A*-*B* molecules would behave qualitatively different than an *A*-*B* mixture. There are no experimental observations demanding that the long-time dynamics is independent of the inertia parameters of the molecules. But we consider the specified isotope effects as artifacts of the approximations underlying the so far studied extensions of MCT. This critique and the formidable complexity of the theories based on the tensor-density descriptions serve as a motivation to search for an alternative approach describing the glassy dynamics of molecular systems. An alternative MCT was proposed by Kawasaki [17]. But so far, nothing is known about the solutions of his equations nor the results concerning the inertia-parameter issue. In this paper the suggestion of Chong and Hirata [18] will be followed, and the MCT will be based on the interaction-site representation of the system [19,20].

The description of a molecular liquid by interaction-site densities is inferior to the one by tensor densities. The correlators of tensor densities can be used to express those of interaction-site densities but not vice versa. Interaction-site theories also have difficulties handling reorientational correlators. Therefore, it is a major goal of this paper to show that the indicated *ad hoc* objections against a MCT based on an interaction-site representation do not fully apply if the theory is restricted to a parameter regime where the cage effect is the dominant mechanism for the dynamics. To proceed, the same dumbbell-molecule problem shall be studied, which was analyzed previously [13,14].

This paper is organized as follows. The basic equations for the model are introduced in Sec. II. Then, the MCT for a diatomic molecule in a simple liquid is formulated in Sec. III. The major problem is the derivation of formulas for the mode-coupling coefficients. This will be done within the Mori-Fujisaka formalism, and the details are presented in Appendix B. In Sec. IV, the results of the theory for the dumbbell in a HSS are discussed. The findings are summarized in Sec. V.

II. THE MODEL

A system of N identical atoms distributed with density ρ at positions $\vec{r}_\kappa, \kappa = 1, \cdots, N$, is considered as solvent. The structure can be described by the density fluctuations for wave vectors $\vec{q}$: $\rho_{\vec{q}} = \Sigma_\kappa \exp(i\vec{q}\cdot\vec{r}_\kappa)$. The structure factor $S_q = \langle |\rho_{\vec{q}}|^2 \rangle / N$ provides the simplest information on the equilibrium distribution of these particles. Here $\langle \cdots \rangle$ denotes canonical averaging for temperature T. Because of isotropy, S_q only depends on the wave number $q = |\vec{q}|$. The Ornstein-Zernike equation, $S_q = 1/[1 - \rho c_q]$, relates S_q to the direct correlation function c_q. The structural dynamics is described in a statistical manner by the normalized density correlators $\phi_q(t) = \langle \rho_{\vec{q}}(t)^* \rho_{\vec{q}} \rangle / N S_q$. They are real even functions of time t and exhibit the initial behavior: $\phi_q(t) = 1 - \frac{1}{2}(\Omega_q t)^2 + O(|t|^3)$. Here $\Omega_q = qv/\sqrt{S_q}$ is the bare phonon dispersion; $v = \sqrt{k_B T/m}$ denotes the thermal velocity of the particles with mass m [20].

A rigid molecule of two atoms A and B shall be considered as solute. Let $\vec{r}_a, a = A$ or B, denote the position vectors of the atoms, so that $L = |\vec{r}_A - \vec{r}_B|$ denotes the distance between the two interaction sites. Vector $\vec{e} = (\vec{r}_A - \vec{r}_B)/L$ abbreviates the axis of the molecule. If m_a denotes the mass of atom a, the total mass $M = m_A + m_B$ and the moment of inertia $I = m_A m_B L^2 / M$ determine the thermal velocities $v_T = \sqrt{k_B T/M}$ and $v_R = \sqrt{k_B T/I}$ for the molecule's translation and rotation, respectively. Let us introduce also the center-of-mass position $\vec{r}_C = (m_A \vec{r}_A + m_B \vec{r}_B)/M$ and the coordinates z_a of the atoms along the molecule axis: $z_A = L(m_B/M)$, $z_B = -L(m_A/M)$. The position of the molecule shall be characterized by the two interaction-site-density fluctuations

$$\rho_{\vec{q}}^a = \exp(i\vec{q}\cdot\vec{r}_a), \quad a = A \text{ or } B. \tag{1}$$

The two-by-two matrix $\mathbf{w}_q$ of static fluctuation correlations $w_q^{ab} = \langle \rho_{\vec{q}}^{a*} \rho_{\vec{q}}^b \rangle$ is given by

$$w_q^{ab} = \delta^{ab} + (1 - \delta^{ab}) j_0(qL), \tag{2}$$

where here and in the following $j_\ell(x)$ denotes the spherical Bessel function of index ℓ. The solute-solvent interaction is described by the pair-correlation function $h_q^a = \langle \rho_{\vec{q}}^* \rho_{\vec{q}}^a \rangle / \rho$, which is expressed by a direct correlation function c_q^a [19]

$$h_q^a = S_q \sum_b w_q^{ab} c_q^b. \tag{3}$$

The dynamics of the molecule shall be characterized by the interaction-site-density correlators

$$F_q^{ab}(t) = \langle \rho_{\vec{q}}^a(t)^* \rho_{\vec{q}}^b \rangle. \tag{4}$$

These are real even functions of time obeying $F_q^{ab}(t) = F_q^{ba}(t)$. They shall be combined to a two-by-two-matrix correlator $\mathbf{F}_q(t)$. Its short-time expansion can be denoted as

$$\mathbf{F}_q(t)=\mathbf{w}_q-\frac{1}{2}q^2\mathbf{J}_q t^2+\mathbf{O}(|t|^3). \tag{5}$$

The continuity equation reads $\dot{\rho}_{\vec{q}}^{a}=i\vec{q}\cdot\vec{j}_{\vec{q}}^{a}$, where the current fluctuation is $\vec{j}_{\vec{q}}^{a}=\vec{v}^a\rho_{\vec{q}}^{a}$, with $\vec{v}^a$ denoting the velocity of atom a. Therefore, one gets $J_q^{ab}=\langle(\vec{q}\cdot\vec{j}_{\vec{q}}^{a})^*(\vec{q}\cdot\vec{j}_{\vec{q}}^{b})\rangle/q^2$. The result splits into a translational and a rotational part, $\mathbf{J}_q=\mathbf{J}_q^{\mathrm{T}}+\mathbf{J}_q^{\mathrm{R}}$, where [21]

$$J_q^{\mathrm{T}ab}=v_{\mathrm{T}}^2 w_q^{ab}, \tag{6a}$$

$$J_q^{\mathrm{R}ab}=v_{\mathrm{R}}^2\left(\frac{2}{3}z_a z_b\right)\{\delta^{ab}+(1-\delta^{ab})[j_0(qL)+j_2(qL)]\}. \tag{6b}$$

Let us denote the small-q expansion of the density correlators in the form

$$F_q^{ab}(t)=1-\frac{1}{6}q^2C^{ab}(t)+O(q^4). \tag{7}$$

The diagonal elements of the symmetric matrix $\mathbf{C}(t)$ are the mean-squared displacements

$$\delta r_a^2(t)=\langle[\vec{r}_a(t)-\vec{r}_a(0)]^2\rangle=C^{aa}(t), \tag{8a}$$

while the off-diagonal elements can be related to the dipole correlator as

$$C_1(t)=\langle\vec{e}(t)\cdot\vec{e}\rangle=\{C^{AB}(t)-\tfrac{1}{2}[C^{AA}(t)+C^{BB}(t)]\}/L^2. \tag{8b}$$

The mean-squared displacement of the center of mass can be expressed as

$$\begin{aligned}\delta r_C^2(t)&=\langle[\vec{r}_C(t)-\vec{r}_C(0)]^2\rangle\\&=[m_A\delta r_A^2(t)+m_B\delta r_B^2(t)]/M+(2I/M)[C_1(t)-1].\end{aligned} \tag{8c}$$

Expanding Eq. (5) in q yields the initial decay

$$\mathbf{C}(t)=\mathbf{C}_0+3\mathbf{J}_0t^2+\mathbf{O}(|t|^3). \tag{9}$$

Here the initial value $\mathbf{C}_0$ is due to the expansion of Eq. (2), while the prefactor of the t^2 term is due to the zero-wave-number limit of Eqs. (6):

$$C_0^{ab}=L^2(1-\delta^{ab}),\quad J_0^{ab}=v_{\mathrm{T}}^2+\frac{2}{3}v_{\mathrm{R}}^2z_a z_b. \tag{10}$$

For symmetric molecules, one gets $m_A=m_B=M/2$, $I=ML^2/4$, and $z_A=-z_B=L/2$. In this case, there are only two independent density correlators, since $F_q^{AA}(t)=F_q^{BB}(t)$. It is convenient to perform an orthogonal transformation to fluctuations of total number densities $\rho_N(\vec{q})$ and ''charge'' densities $\rho_Z(\vec{q})$:

$$\rho_x(\vec{q})=(\rho_{\vec{q}}^{A}\pm\rho_{\vec{q}}^{B})/\sqrt{2},\quad x=N\ \text{or}\ Z. \tag{11a}$$

The transformation matrix $\mathbf{P}=\mathbf{P}^{-1}$ reads

$$\mathbf{P}=\frac{1}{\sqrt{2}}\begin{pmatrix}1 & 1\\ 1 & -1\end{pmatrix}. \tag{11b}$$

It diagonalizes the matrices $\mathbf{w}_q$ from Eq. (2) and $\mathbf{J}_q$ from Eqs. (6):

$$(\mathbf{P}\mathbf{w}_q\mathbf{P})^{xy}=\delta^{xy}w_x(q),\quad w_x(q)=1\pm j_0(qL), \tag{11c}$$

$$(\mathbf{P}\mathbf{J}_q^{\mathrm{T}}\mathbf{P})^{xy}=\delta^{xy}v_{\mathrm{T}}^2w_x(q), \tag{11d}$$

$$(\mathbf{P}\mathbf{J}_q^{\mathrm{R}}\mathbf{P})^{xy}=\delta^{xy}\frac{1}{6}v_{\mathrm{R}}^2L^2\{1\mp[j_0(qL)+j_2(qL)]\}, \tag{11e}$$

where $x,y=N$ or Z. Also, the matrix of density correlators is diagonalized. Introducing the normalized correlators $\phi_q^x(t)$, one gets

$$\begin{aligned}\phi_q^x(t)&=\langle\rho_x(\vec{q},t)^*\rho_x(\vec{q})\rangle/w_x(q),\\ [\mathbf{P}\mathbf{F}_q(t)\mathbf{P}]^{xy}&=\delta^{xy}\phi_q^x(t)w_x(q).\end{aligned} \tag{12}$$

The mean-squared displacements are equal and shall be denoted by $\delta r^2(t)=\delta r_A^2(t)=\delta r_B^2(t)$, so that Eq. (8c) reads $\delta r^2(t)=\delta r_C^2(t)+(1/2)L^2[1-C_1(t)]$. The matrix $\mathbf{C}(t)$ is diagonalized:

$$[\mathbf{P}\mathbf{C}(t)\mathbf{P}]^{NN}=2\,\delta r_C^2(t)+L^2,\quad [\mathbf{P}\mathbf{C}(t)\mathbf{P}]^{ZZ}=-L^2C_1(t). \tag{13}$$

In Appendix A we show how the correlation functions in the interaction-site representation can be expressed in terms of the ones in the tensor-density representation.

III. APPROXIMATIONS

A. The solvent-density correlator

The density correlator of the solvent is needed to formulate the equations for the probe molecule. This quantity is discussed comprehensively in the preceding literature on the MCT for simple systems [22]. Let us note here only those equations that have to be solved in order to obtain the input information for the calculations of the present paper. First, there is the exact Zwanzig-Mori equation of motion [20] relating the correlator for density fluctuations $\phi_q(t)$ to the correlator $m_q(t)$ for the force fluctuations:

$$\partial_t^2\phi_q(t)+\Omega_q^2\phi_q(t)+\Omega_q^2\int_0^t dt'\,m_q(t-t')\,\partial_{t'}\phi_q(t')=0. \tag{14}$$

Second, there is the approximate expression for kernel $m_q(t)$ as mode-coupling functional

$$m_q(t)=\mathcal{F}_q[\phi(t)]. \tag{15a}$$

The functional $\mathcal{F}_q$ is rederived as Eq. (B11) in Appendix B. The wave numbers are discretized to M values with spacing h: $q/h=1/2,3/2,\cdots,M-1/2$. Then $\phi(t)$ and similar quantities are to be viewed as vectors of M components $\phi_q(t)$, $q=1,\cdots,M$, and the functional is

$$\mathcal{F}_q[\tilde{f}] = \sum_{kp} V_{q,kp} \tilde{f}_k \tilde{f}_p . \tag{15b}$$

Third, Eqs. (14) and (15a) imply the equation for the long-time limit $f_q = \phi_q(t \to \infty)$:

$$f_q = \mathcal{F}_q[f]/\{1 + \mathcal{F}_q[f]\}. \tag{16}$$

For the liquid state, there is only the trivial solution $f_q = 0$. The glass is characterized by a nonergodicity parameter $0 < f_q < 1$, which has the meaning of the Debye-Waller factor of the arrested structure. At the liquid-glass transition, the long-time limit of the correlator changes discontinuously from zero to the critical value $f_q^c > 0$.

B. The solute-interaction-site-density correlators

For matrices of correlation functions as defined in Eq. (4), the Zwanzig-Mori formalism also leads to an exact equation of motion [20]:

$$\partial_t^2 \mathbf{F}_q(t) + \mathbf{\Omega}_q^2 \mathbf{F}_q(t) + \mathbf{\Omega}_q^2 \int_0^t dt' \mathbf{m}_q(t-t') \partial_{t'} \mathbf{F}_q(t') = \mathbf{0}. \tag{17a}$$

From the short-time expansion together with Eq. (5), one gets

$$\mathbf{\Omega}_q^2 = q^2 \mathbf{J}_q \mathbf{w}_q^{-1} . \tag{17b}$$

The right-hand side (rhs) of this equation is a product of two symmetric positive definite matrices. Hence it can be written as the square of a matrix $\mathbf{\Omega}_q$. Splitting off this matrix before the convolution integral is done for later convenience.

The difficult problem is deriving an approximation for the matrix $\mathbf{m}_q(t)$ of fluctuating-force correlations such that the cage effect is treated reasonably. The result, Eq. (B17) from Appendix B, can be formulated as mode-coupling functional $\boldsymbol{\mathcal{F}}_q$:

$$m_q^{ab}(t) = \mathcal{F}_q^{ab}[\mathbf{F}(t), \phi(t)]. \tag{18a}$$

After the discretization of the wave numbers as explained above, $\boldsymbol{\mathcal{F}}_q$ reads

$$\mathcal{F}_q^{ab}[\tilde{\mathbf{f}}, \tilde{f}] = q^{-2} \sum_c w_q^{ac} \sum_{kp} V_{q,kp}^{cb} \tilde{f}_k^{cb} \tilde{f}_p . \tag{18b}$$

The preceding equations are matrix generalizations of the MCT equations for the tagged-particle-density correlator $\phi_q^s(t)$ in a simple liquid [23].

The equation for the nonergodicity parameters of the molecule, $F_q^{ab\infty} = F_q^{ab}(t \to \infty)$, can be obtained from Eqs. (17a) and (18a). It is a matrix generalization of Eq. (16):

$$\mathbf{F}_q^{\infty} = \boldsymbol{\mathcal{F}}_q[\mathbf{F}^{\infty}, f]\{\mathbf{1} + \boldsymbol{\mathcal{F}}_q[\mathbf{F}^{\infty}, f]\}^{-1} \mathbf{w}_q . \tag{19}$$

If the solvent is a liquid, i.e., if $f_q = 0$, one gets $\mathbf{F}_q^{\infty} = \mathbf{0}$. If the solvent is a glass, the long-time limits $F_q^{ab\infty}$ can be nontrivial. In this case, the solvent properties enter via the Debye-Waller factors f_q, which renormalize the coupling coefficients $V_{q,kp}^{cb}$ in Eq. (18b).

Let us specialize to symmetric molecules. Multiplying Eqs. (17)–(19) from left and right with $\mathbf{P}$ given by Eq. (11b) and inserting $\mathbf{1} = \mathbf{PP}$ between every pair of matrices, all equations are transformed into diagonal ones. Thus, there are two equations of motion,

$$\partial_t^2 \phi_q^x(t) + \Omega_q^{x2} \phi_q^x(t) + \Omega_q^{x2} \int_0^t dt' m_q^x(t-t') \partial_{t'} \phi_q^x(t') = 0, \qquad x = N \text{ or } Z. \tag{20}$$

The two characteristic frequencies Ω_q^x, which specify the initial decay of the correlators by $\phi_q^x(t) = 1 - \frac{1}{2}(\Omega_q^x t)^2 + O(|t|^3)$, read

$$\Omega_q^{N2} = (v_T q)^2 + \frac{1}{6}(v_R L q)^2 \times [1 - j_0(qL) - j_2(qL)]/[1 + j_0(qL)], \tag{21a}$$

$$\Omega_q^{Z2} = (v_T q)^2 + \frac{1}{6} v_R^2 [1 + j_0(qL) + j_2(qL)] \times (qL)^2/[1 - j_0(qL)]. \tag{21b}$$

The relaxation kernels can be written as $m_q^x(t) = \mathcal{F}_q^x[\phi^x(t), \phi(t)]$, where Eq. (B17) gives

$$\mathcal{F}_q^x[\tilde{f}^x, \tilde{f}] = [w_x(q)/q^2] \int \frac{d\vec{k}}{2(2\pi)^3} (\vec{q} \cdot \vec{p}/q)^2 \times w_x(k) \rho S_p c^N(p)^2 \tilde{f}_k^x \tilde{f}_p . \tag{22a}$$

Here $\vec{p} = \vec{q} - \vec{k}$, and $c^N(p) = \sqrt{2} c_p^A = \sqrt{2} c_p^B$. The above specified discretization of the wave numbers yields $\mathcal{F}_q^x$ as polynomial

$$\mathcal{F}_q^x[\tilde{f}^x, \tilde{f}] = [w_x(q)/q^2] \sum_{kp} V_{q,kp}^x \tilde{f}_k^x \tilde{f}_p . \tag{22b}$$

One gets for the nonergodicity parameters $f_q^x = \phi_q^x(t \to \infty) = (F_q^{AA\infty} \pm F_q^{AB\infty})/w_x(q)$

$$f_q^x = \mathcal{F}_q^x[f^x, f]/\{1 + \mathcal{F}_q^x[f^x, f]\}. \tag{23}$$

There is no coupling between the fluctuations of the total density and those of the charge density. The mathematical structure of the two sets of equations for $x = N$ and $x = Z$, respectively, is the same as the one studied previously for the density correlator $\phi_q^s(t)$ of a tagged particle in a simple liquid [23]. For the density dynamics one also finds the small-q asymptote for the frequency $\Omega_q^{N2} = (v_T q)^2 + O(q^4)$, reflecting free translation of the probe molecule. There is also the q^{-2} divergency of the mode-coupling coefficients in $\mathcal{F}_q^N$, which implies the approach towards unity of the Lamb-Mössbauer factor for vanishing wave number: $f_{q \to 0}^N = 1$. For

the charge dynamics, one gets a nonzero small-q limit for the frequency characterizing free rotation $\Omega^{Z2}_{q\to 0}=2v_R^2+O(q^2)$. The mode-coupling coefficients do not diverge for $q\to 0$, since $6w_Z(q)/(Lq)^2\to 1$. Therefore, the nonergodicity parameter for the variable $\rho_Z(\vec{q},t)$ approaches a limit smaller than unity: $f^Z_{q\to 0}<1$.

C. The dipole correlator and the mean-squared displacements

According to Eqs. (8), the knowledge of the dipole correlator $C_1(t)$ and two of the mean-squared displacements $\delta r_a^2(t)$ for $a=A$, B, or C is equivalent to the knowledge of the three independent elements of the symmetric matrix $\mathbf{C}(t)$. Using Eq. (7) and expanding Eq. (17a) for small wave numbers, one gets

$$\partial_t^2\mathbf{C}(t)-\mathbf{D}+\mathbf{\Omega}_0^2\mathbf{C}(t)+\mathbf{J}_0\int_0^t dt'\mathbf{m}(t-t')\partial_{t'}\mathbf{C}(t')=\mathbf{0}. \tag{24}$$

This exact equation of motion for $\mathbf{C}(t)$ has to be solved with the initial condition from Eq. (9). The frequency matrix is obtained as zero-wave-number limit from Eq. (17b)

$$\mathbf{\Omega}_0^2=(2v_R^2/L)\begin{pmatrix} z_A & -z_A \\ z_B & -z_B\end{pmatrix}. \tag{25}$$

Equation (24) implies $\ddot{\mathbf{C}}(0)-\mathbf{D}+\mathbf{\Omega}_0^2\mathbf{C}(0)=\mathbf{0}$. Thus, one gets from Eq. (9) $\mathbf{D}=6\mathbf{J}_0+\mathbf{\Omega}_0^2\mathbf{C}_0$, i.e., $D^{ab}=6v_T^2+2v_R^2(z_A+z_B)z_a$.

The MCT approximation for the kernel $\mathbf{m}(t)$ is obtained by combining Eqs. (17b) and (18b) and taking the zero-wave-vector limit. With Eq. (B17), one finds

$$\mathbf{m}(t)=\boldsymbol{\mathcal{F}}[\mathbf{F}(t),\phi(t)], \tag{26a}$$

$$\mathcal{F}^{ab}[\tilde{\mathbf{f}},\tilde{f}]=\frac{1}{6\pi^2}\int_0^\infty dkk^4\rho S_k c_k^a c_k^b \tilde{f}_k^{ab}\tilde{f}_k. \tag{26b}$$

Again, the theory simplifies considerably for symmetric molecules. In this case, one can transform Eq. (24) as explained in connection with the derivation of Eq. (20). Using Eq. (13) one gets the exact equation of motion for the mean-squared displacement

$$\partial_t^2\delta r_C^2(t)-6v_T^2+v_T^2\int_0^t dt' m_N(t-t')\partial_{t'}\delta r_C^2(t')=0, \tag{27}$$

to be solved with the initial behavior $\delta r_C^2(t)=3(v_Tt)^2+O(|t|^3)$. Similarly, one obtains for the dipole correlator

$$\partial_t^2 C_1(t)+2v_R^2C_1(t)+2v_R^2\int_0^t dt' m_Z(t-t')\partial_{t'}C_1(t')=0, \tag{28}$$

to be solved with the initial decay $C_1(t)=1-(v_Rt)^2+O(|t|^3)$. The MCT approximation for the kernels is obtained from Eq. (26b):

$$m_x(t)=\mathcal{F}_x[\phi^x(t),\phi(t)],\quad x=N \text{ or } Z, \tag{29a}$$

$$\mathcal{F}_x[\tilde{f}^x,\tilde{f}]=\alpha_x\int_0^\infty dkk^4\rho S_k c^N(k)^2 w_x(k)\tilde{f}_k^x\tilde{f}_k, \tag{29b}$$

where $\alpha_N=1/(6\pi^2)$ and $\alpha_Z=L^2/(72\pi^2)$. Equations (28) and (29) for the dipole correlator have the standard form of the MCT equation. If $\phi_q^Z(t)$ approaches zero for large times, the same approach towards equilibrium is exhibited by $C_1(t)$. If the solvent is a glass, $f_q>0$, and if the charge-density fluctuations $\phi_q^Z(t)$ exhibit nonergodic behavior, $f_q^Z>0$, the $\ell=1$-reorientational correlator also exhibits nonergodic dynamics:

$$C_1(t\to\infty)=f_1=\mathcal{F}_Z[f^Z,f]/\{1+\mathcal{F}_Z[f^Z,f]\}. \tag{30}$$

Parameter f_1 is the long-wavelength limit of f_q^Z discussed in Eq. (23): $f^Z_{q\to 0}=f_1$.

D. The quadrupole correlator

The quadrupole correlator $C_2(t)=\langle 3[\vec{e}(t)\cdot\vec{e}]^2-1\rangle/2$ cannot be extracted from the correlators $F_q^{ab}(t)$ with $a,b=A$ or B. But let us consider a linear symmetric triatomic molecule. The third atom, labeled C, has its position in the center $\vec{r}_C$. The preceding theory can be extended by adding as a third variable the fluctuations $\rho_q^C=\exp(i\vec{q}\cdot\vec{r}_C)$. The basic quantities are now the elements of the 3×3 matrix correlator, defined as in Eq. (4) with $a,b=A$, B, or C. The correlator formed with $\rho_Q(\vec{q})=\rho_{\vec{q}}^A+\rho_{\vec{q}}^B-2\rho_{\vec{q}}^C$ is a linear combination of the nine functions $F_q^{ab}(t)$. An expansion for small q yields

$$\langle\rho_Q(\vec{q},t)^*\rho_Q(\vec{q})\rangle=\frac{1}{180}(qL)^4\left[C_2(t)+\frac{5}{4}\right]+O(q^6). \tag{31}$$

In this case, $C_2(t)$ can be obtained in a manner similar to that discussed above for $C_1(t)$. A diatomic molecule can be considered a special mathematical limit of a triatomic one. Hence, there is, in principle, no problem obtaining $C_2(t)$ within a theory based on an interaction-site description. Motivated by this observation, an auxiliary site C shall be introduced [24,25] and $\rho_{\vec{q}}^C$ will be used as the third basic variable. However, a complete theory with 3×3 matrices shall not be developed. Rather, some additional approximations will be introduced so that $C_2(t)$ is obtained as a corollary of the above-formulated closed theory.

The quadrupole correlator can be written as the small-q limit of a correlation function formed with tensor-density fluctuations defined in Eq. (A1) for $\vec{q}_0=(0,0,q)$: $C_2(t)=\lim_{q\to 0}\langle\rho_2^0(\vec{q}_0,t)^*\rho_2^0(\vec{q}_0)\rangle$. Therefore, an exact Zwanzig-Mori equation can be derived as usual:

$$\partial_t^2 C_2(t)+6v_R^2C_2(t)+6v_R^2\int_0^t dt' m_2^R(t-t')\partial_{t'}C_2(t')=0. \tag{32}$$

The relaxation kernel $m_2^{\mathrm{R}}(t)$ is a correlator for fluctuating forces $F_{\mathrm{R}2}(q0,t)$ referring to angular-momentum index $\ell=2$ and helicity $m=0$:

$$m_2^{\mathrm{R}}(t)=\lim_{q\to 0}\langle F_{\mathrm{R}2}(q0,t)^* F_{\mathrm{R}2}(q0)\rangle. \tag{33}$$

The time evolution of the fluctuating force is generated by the reduced Liouvillian $\mathcal{L}'=\mathcal{Q}L\mathcal{Q}$, where $\mathcal{Q}$ projects perpendicular to $\rho_2^0(\vec{q}_0)$ and $\mathcal{L}\rho_2^0(\vec{q}_0)$, and the Liouvillian $\mathcal{L}$ is defined by $i\mathcal{L}A(t)=\partial_t A(t)$. The notation has been chosen so as to bring the formulas into agreement with those of the more general theory in Ref. [13]. The procedure used for the theory of simple liquids [26] shall be applied to derive an approximation for the kernel. First, the forces will be approximated by the projection onto the space of the simplest modes contributing $F_{\mathrm{R}2}\to\mathcal{P}'F_{\mathrm{R}2}$. Here $\mathcal{P}'$ projects onto the space spanned by the pair modes

$$A^a(\vec{k},\vec{p})=\rho^a_{\vec{k}}\rho_{\vec{p}}/\sqrt{NS_p},\quad a=A,\ B,\ \text{or}\ C. \tag{34a}$$

The essential step is the second one, where correlations of the pairs are replaced by products of correlations:

$$\langle A^a(\vec{k},\vec{p},t)^* A^{a'}(\vec{k}',\vec{p}')\rangle\to\delta_{\vec{k}\vec{k}'}\delta_{\vec{p}\vec{p}'}\langle\rho^a_{\vec{k}}(t)^*\rho^{a'}_{\vec{k}}\rangle \times\langle\rho_{\vec{p}}(t)^*\rho_{\vec{p}}\rangle/NS_p.$$

This approximation is done in particular for $t=0$, thereby deriving for the normalization matrix for the pair modes $\langle A^a(\vec{k},\vec{p})^* A^b(\vec{k}',\vec{p}')\rangle\to\delta_{\vec{k}\vec{k}'}\delta_{\vec{p}\vec{p}'}w_k^{ab}$. Here $w^{ab}(k)=j_0[k(z_a-z_b)]$ generalizes Eq. (2) to a 3×3 matrix. As a result, one gets

$$\begin{aligned} m_2^{\mathrm{R}}(t)=\lim_{q\to 0}\sum_{\vec{k}\vec{p}}\sum_{abcd}&\langle F_{\mathrm{R}2}(q0)^* A^a(\vec{k},\vec{p})\rangle\\ &\times(\mathbf{w}_k^{-1})^{ab}F_k^{bc}(t)\phi_p(t)\\ &\times(\mathbf{w}_k^{-1})^{cd}\langle A^d(\vec{k},\vec{p})^* F_{\mathrm{R}2}(q0)\rangle. \end{aligned}\tag{34b}$$

The $q\to 0$ limit is carried out easily, reducing the sum over $\vec{k}$ and $\vec{p}$ to the one over $\vec{k}$ with $\vec{k}=-\vec{p}$. One obtains the kernel as mode-coupling functional

$$m_2^{\mathrm{R}}(t)=\int_0^\infty dk\sum_{ab\in\{A,B,C\}}V_2^{ab}(k)F_k^{ab}(t)\phi_k(t). \tag{35}$$

Let us restrict the discussion to symmetric molecules. For this case, an explicit expression for $V_2^{ab}(k)$ is noted as Eqs. (A9) in Appendix A.

The correlators $\phi_k(t)$ and $F_k^{ab}(t)$ with $a,b=A$ or B are taken from Secs. III A and III B, respectively. The theory of Sec. III C provides the results for the mean-squared displacement $\delta r_C^2(t)$. The Gaussian approximation shall be used to evaluate $F_k^{CC}(t)\approx\exp[-\frac{1}{6}k^2\delta r_C^2(t)]$. The two remaining functions can be expressed in terms of tensor-density fluctuations according to Eq. (A6): $F_k^{aC}(t)=\Sigma_\ell\sqrt{(2\ell+1)}j_\ell(kz_a)\phi_{\ell 0}(k0,t)$ for $a=A$ or B. As in the previous work [14], only the diagonal correlators shall be taken in the sum, i.e., the approximation will be used: $F_k^{aC}(t)\approx j_0(kz_a)F_k^{CC}(t)$.

IV. RESULTS

A few concepts shall be mentioned which were introduced [26] to describe the MCT-liquid-glass-transition dynamics. In the space of control parameters, a smooth function σ is defined near the transition points, called the separation parameter. Glass states are characterized by $\sigma>0$, liquid states by $\sigma<0$, and $\sigma=0$ defines the transition hypersurface. Suppose only one control parameter, say, the density ρ, is varied near the transition point. Then one can write for small distance parameters $\epsilon=(\rho-\rho_c)/\rho_c:\sigma=C\epsilon$, $C>0$. In addition to C, the transition point is characterized by a time scale t_0 and by a number λ, $0<\lambda<1$. The scale t_0 specifies properties of the transient dynamics, and λ is called the exponent parameter. The latter determines a certain number $B>0$, the critical exponent a, $0<a\leqslant 1/2$, and the von Schweidler exponent b, $0<b\leqslant 1$. There are two critical time scales governing the bifurcation dynamics close to the transition:

$$t_\sigma=t_0/|\sigma|^\delta,\quad t'_\sigma=t_0B^{-1/b}/|\sigma|^\gamma. \tag{36}$$

The anomalous exponents of the scales read $\delta=1/2a$, $\gamma=1/2a+1/2b$. The HSS shall be used as solvent. There is only one control parameter for the equilibrium structure, which shall be chosen as the packing fraction φ of the particles with diameter d, $\varphi=\pi\rho d^3/6$. The distance parameter shall be given by the logarithm x of $|\epsilon|$:

$$\epsilon=(\varphi-\varphi_c)/\varphi_c=\pm 10^{-x}. \tag{37}$$

The structure factor S_q is calculated within the Percus-Yevick theory [20]. The wave numbers are discretized to $M=100$ values with spacing $hd=0.4$. For this solvent model, results for the density correlators and their spectra can be found in Ref. [27]. The glassy dynamics is analyzed in Ref. [22], from which one infers $\varphi_c=0.516$, $C=1.54$, $\lambda=0.735$, $a=0.312$, $b=0.583$, and $B=0.836$. Furthermore, $t_0=0.0236(d/v)$ [15].

Dumbbells of two fused hard spheres of diameters $d_A=d_B=d$ shall be used as solute. The elongation parameter $\zeta=L/d$ quantifies the bond length. The solute-solvent-direct-correlation functions are also calculated within the Percus-Yevick theory. Within the tensor-density description, the direct correlation functions $c_\ell(q)$ have been determined in Ref. [28]. These results are substituted in the formulas of Appendix A, to evaluate the equilibrium structure in the site representation. In all summations over contributions due to various angular-momentum indices ℓ, a cutoff $\ell_{co}=8$ is chosen. It was checked for representative cases that increasing the cutoff to $\ell_{co}=16$ does not significantly change the results to be discussed. The discretization of the various wave-vector integrals is done as specified above for the solvent. The results in Secs. IV A and IV B deal with a sym-

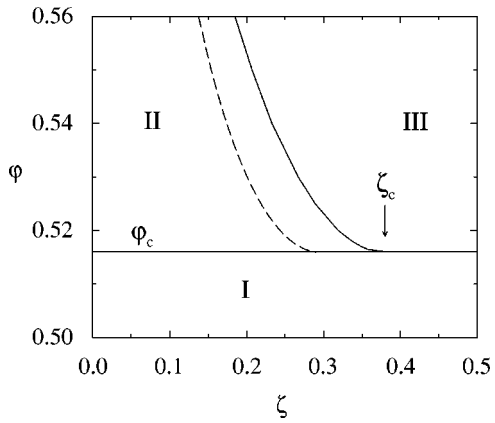

FIG. 1. Phase diagram of a dilute solute of symmetric dumbbell molecules with elongation ζ consisting of two fused hard spheres immersed in a hard-sphere system with packing fraction φ. The horizontal line marks the liquid-glass transition at the critical packing fraction $\varphi_c=0.516$. The other full line is the curve $\zeta_c(\varphi)$ of critical elongations for a type-*A* transition between phases II and III. In phase II dipole fluctuations of the solute relax to zero for long times, while they are frozen in phase III. The value $\zeta_c=\zeta_c(\varphi_c)=0.380$ is marked by an arrow. The dashed line is the corresponding transition curve calculated in Ref. [29]; it terminates at $\zeta_c^t=0.297$.

metric dumbbell with $m_A=m_B=m$, and in Sec. IV C the molecule with $m_A=10m$, $m_B=m$ is considered.

Throughout the rest of this paper, the particle diameter is chosen as unit of length, $d=1$, and the unit of time is chosen so that the thermal velocity of the solvent is $v=1$.

A. Structural arrest

There are two control parameters for the system, namely, the packing fraction φ of the solvent and the elongation ζ of the solute molecule. Figure 1 exhibits the phase diagram. Phase I deals with states where φ is below the critical value φ_c, i.e., the solvent is a liquid. In this case, the long-time limits of the mode-coupling kernels in Eqs. (18) vanish. All solute correlators relax to zero for long times, and the molecule diffuses through the solvent. For $\varphi\geqslant\varphi_c$, the solvent is a glass. Structural fluctuations behave nonergodically. In particular, a tagged solvent particle does not diffuse; rather, it is localized. Since the atoms of the molecule with $d_A=d_B=d$ experience the same interaction with the solvent as the solvent particles do among each other, one expects the molecule to be localized as well. Indeed, Eq. (23) yields for $\varphi\geqslant\varphi_c$: $f_q^N>0$. If φ increases from below φ_c to above φ_c, the long-time limit $\phi_q^N(t\rightarrow\infty)$ increases discontinuously at φ_c from zero to $f_q^{Nc}>0$. Also, the quadrupole correlator exhibits nonergodic dynamics: $C_2(t\rightarrow\infty)=f_2>0$. The cages surrounding the molecule cause such strong steric hindrance that quadrupole fluctuations of the orientational vector $\vec{e}$ cannot relax to zero. In this sense, the states $\varphi\geqslant\varphi_c$ are ideal glasses.

There are two alternatives for the glass. Phase II deals with states for sufficiently small ζ. There is such small steric hindrance for a flip of the molecule's axis between the two energetically equivalent positions $\vec{e}$ and $-\vec{e}$ that Eq. (23) yields $f_q^Z=0$. The dynamics of the charge fluctuations is ergodic. In particular, the dipole correlator relaxes to zero: $C_1(t\rightarrow\infty)=0$. Phase II is an amorphous counterpart of a plastic crystal. For sufficiently large ζ, steric hindrance for dipole reorientations is so effective, that the charge fluctuations also behave nonergodically. In this case, Eq. (23) yields a positive long-time limit $0<f_q^Z=\phi_q^Z(t\rightarrow\infty)$. In particular, dipole-disturbances do not relax to zero: $C_1(t\rightarrow\infty)=f_1>0$. This phase, III, is a glass with all structural disturbances exhibiting nonergodic motion. Phases II and III are separated by transitions at $\zeta=\zeta_c(\varphi)$, $\varphi\geqslant\varphi_c$. With decreasing density, the steric hindrance for reorientations decreases. Thus, $\zeta_c(\varphi)$ increases with decreasing φ, as shown by the full line in Fig. 1. The transition curve terminates with a horizontal slope at the largest critical elongation $\zeta_c=\zeta(\varphi_c)=0.380$. Function $\zeta_c(\varphi)$ was calculated before within the MCT based on the tensor-density description [29], and the transition curve of this theory is added as a dashed line in Fig. 1. The results of the two theories are in qualitative agreement. It would be interesting if molecular-dynamics studies could determine, which of the two theories is closer to reality. The asymptotic laws for the transition from phase II to phase III have previously been described as a type-*A* transition, as can be inferred from Ref. [30] and the papers quoted there. At this transition, $C_1(t\rightarrow\infty)$ increases continuously with increasing ζ.

The heavy full lines in Fig. 2 exhibit critical nonergodicity parameters f_q^{xc} for $\zeta=0.80$, calculated from Eq. (23) for the liquid-glass transition point $\varphi=\varphi_c$. These quantities are Lamb-Mössbauer factors of the molecule. The function f_q^{Nc} can be measured, in principle, as a cross section for incoherent neutron scattering from the solute, provided both centers *A* and *B* are identical atoms without spin. As expected for a localized probability-distribution Fourier transform, the f_q^{xc}-versus-q curves decrease with increasing q. Most remarkable are the kinks exhibited by f_q^{Nc} for wave numbers q near 5, 12.5, and 20, and by f_q^{Zc} for q near 10 and 17.5. The light full lines exhibit f_q^{xc} calculated with Eq. (A7) from the critical nonergodicity parameters $f^c(q\ell 0)$ [13]. The results of both approximation theories are in semiquantitative agreement, in particular concerning the position and size of the kinks. The $f^c(q\ell 0)$-versus-q curves are bell shaped, close to Gaussians [13]. They enter into Eq. (A7) with prefactors $j_\ell(q\zeta/2)^2=O(q^{2\ell})$, so that the maximum of the contribution from angular-momentum index ℓ occurs at some $q_\ell^{\max}$ that increases with ℓ. The separate contributions for different ℓ are shown as dotted lines in Fig. 2. Thus, the kinks are due to interference effects of the $f^c(q\ell 0)$ with the intramolecular form factors $j_\ell(q\zeta/2)$. Let us add that also the Lamb-Mössbauer factors of the atoms, f_q^{ac}, are well described by Gaussians for $q<10$; in particular, these functions do not exhibit kinks. Figure 2 demonstrates for a case of strong steric hindrance for reorientational motion that angular-momentum variables for ℓ up to 6 are relevant in describing the arrested structure, and that the description of the molecule by site-density fluctuations properly accounts for the contributions with $\ell\geqslant 2$.

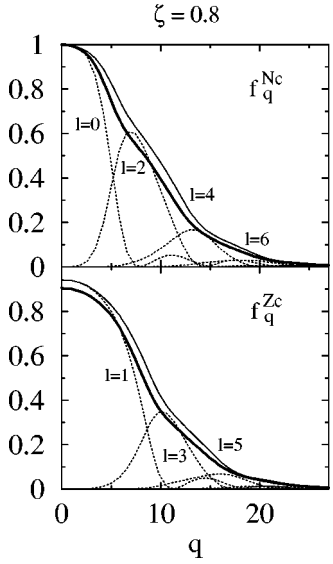

FIG. 2. Nonergodicity parameters f_q^{xc} (heavy full lines) for the molecule's arrested number-density fluctuations ($x=N$) and charge-density fluctuations ($x=Z$) for the critical packing fraction $\varphi=\varphi_c$. The elongation parameter $\zeta=0.80$ is representative for strong steric hindrance for reorientational motion. The light full lines are evaluated with Eq. (A7) with the nonergodicity parameters $f^c(q\ell 0)$ obtained in Ref. [13] from a theory based on a tensor-density description. The dotted lines show the contributions to Eq. (A7) from different angular-momentum index ℓ. Here and in the following figures the diameter of the spheres is used as unit of length, $d=1$.

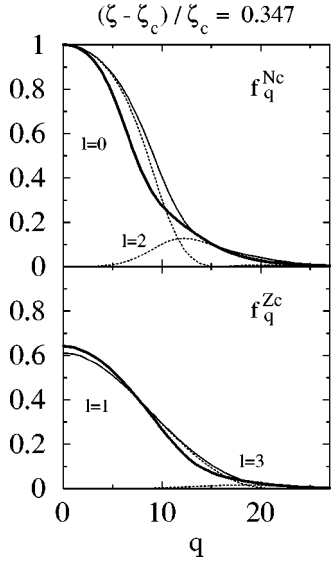

FIG. 3. Results as in Fig. 2 but for small elongations which are representative for weak steric hindrance for reorientational motion. The relative distance from the transition point between phases II and III is $(\zeta-\zeta_c)/\zeta_c=0.347$. The heavy full line shows the result of the present theory for $\zeta=0.512$. The light full line shows the result for $\zeta=0.400$ based on Ref. [13].

Figure 3 exhibits f_q^{xc} representative for weak steric hindrance for the reorientational dynamics. Naturally, the contributions due to the arrest of fluctuations of tensor densities with large ℓ are suppressed. The contributions for $\ell=0$ and $\ell=2$ are sufficient to explain f_q^{Nc}, in particular its kink for q near 12.5. Similarly, the contributions for $\ell=1$ and $\ell=3$ are necessary and sufficient to explain f_q^{Zc} with its kink for q near 17.5. The dynamics is strongly influenced by precursor phenomena of the transition from phase II to phase III. This is demonstrated, for example, by the strong decrease of $f_1^c=f_{q\to 0}^{Zc}$ for the result shown in the lower panel of Fig. 3 in comparison to the one shown in the lower panel of Fig. 2. The two approximation theories under discussion yield different numbers for the value ζ_c for the transition point. It is meaningless to compare different approximations for results near a singularity ζ_c, referring to the same value ζ. It is more meaningful to compare results for the same relative distance from the critical point, $(\zeta-\zeta_c)/\zeta_c$, as is done in Fig. 3. Let us mention that f_q^{Zc} shown by the heavy and light full lines would be somewhat closer, if one had compared elongations yielding the same value for f_1^c.

Figure 4 exhibits critical Lamb-Mössbauer factors f_q^{xc} as a function of the elongation. The lower panel demonstrates the transition from phase II for $\zeta<\zeta_c$ to phase III for $\zeta>\zeta_c$. For strong steric hindrance, say, $\zeta\geqslant 0.8$, f_q^{Nc} is rather close to f_q^{Zc} provided q is not too small, say, $q>3$. For ζ approaching ζ_c, the f_q^{Zc} fall below f_q^{Nc}. Most remarkable are the wiggles or even minima of the curves. These are the analogues of the kinks, discussed above in connection with Figs. 2 and 3. Again, these anomalies can be explained as interference effects between the geometric structure factors $j_\ell(q\zeta/2)^2$ and the nonergodicity parameters $f^c(q\ell 0)$ according to Eq. (A7). Let us consider f_q^{Nc} for an intermediate wave vector as shown for curves b and c in the upper panel of Fig. 4. For small ζ, say, $\zeta\leqslant 0.4$, the $\ell=0$ contribution dominates the sum in Eq. (A7), as can be inferred from Fig. 3. Function $f^c(q00)$ reflects the isotropic part of the arrested fluctua-

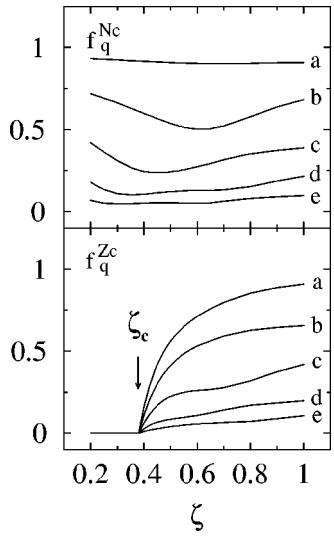

FIG. 4. Critical nonergodicity parameters f_q^{xc} for the solute as a function of the elongation parameter ζ for the wave numbers $q=3.4(a)$, $7.0(b)$, $10.6(c)$, $14.2(d)$, and $17.4(e)$. The arrow marks the transition point from phase II to phase III at $\zeta_c=0.380$.

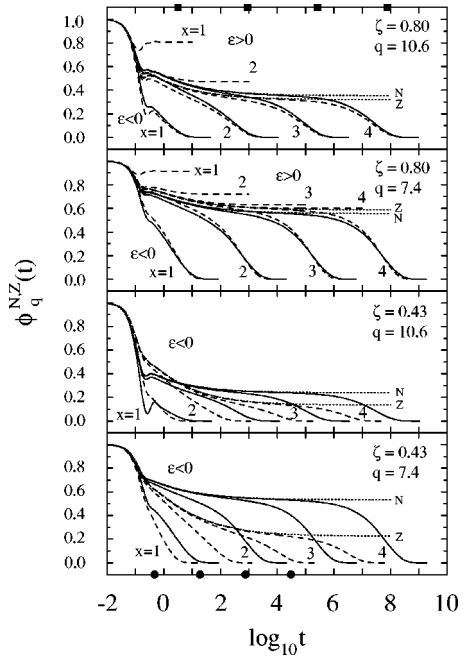

FIG. 5. Correlators $\phi_q^N(t)$ (solid lines) and $\phi_q^Z(t)$ (dashed lines) for two intermediate wave numbers q as a function of the logarithm of time t. The decay curves at the critical packing fraction φ_c for number-density and charge-density correlators are shown as dotted lines and marked by N and Z, respectively. Only a few solutions of glass states are shown for $\phi_q^Z(t)$ in order to avoid overcrowding the figure. The distance parameter is $\epsilon=(\varphi-\varphi_c)/\varphi_c=\pm 10^{-x}$. The full circles and squares mark the characteristic times t_σ and t'_σ, respectively, according to Eq. (36) for $x=1$, 2, 3, and 4. The unit of time is chosen here and in the following figures such that the thermal velocity of the solvent reads $v=1$.

tions, and hence it is practically ζ independent (as shown in Fig. 5 of Ref. [13]). Since $j_0(q\zeta/2)^2=1-\frac{1}{12}(q\zeta)^2+O[(q\zeta)^4]$ decreases with increasing ζ, the f_q^{Nc} versus ζ curve decreases too; and the decrease is stronger for larger q. The $f^c(q20)$ increase from 0 for $\zeta=0$ to values near 0.5 for $\zeta=1$ (as shown in Fig. 5 of Ref. [13]). Also, the geometric structure factor increases strongly with ζ: $j_2(q\zeta/2)^2=[(q\zeta)^2/60]^2+O[(q\zeta)^6]$. The combined effect of both increases causes the increase of the f_q^{Nc}-versus-ζ curve for larger ζ. The resulting minimum occurs for smaller ζ if q is larger, and this explains the difference between the two curves b and c. The theory produces the minima, since it accounts for the arrest of tensor-density fluctuations for $\ell \geqslant 2$.

B. Correlation functions and spectra near the glass transition

Figure 5 demonstrates the evolution of the dynamics for the correlators $\phi_q^N(t)$ and $\phi_q^Z(t)$ for intermediate wave numbers q near the transition from phase I to phase III. The oscillatory transient dynamics occurs within the short-time window $t<1$. The control-parameter sensitive glassy dynamics occurs for longer times for packing fractions φ near φ_c. At the transition point $\varphi=\varphi_c$, the correlators decrease in a stretched manner towards the plateau values f_q^{xc} as shown by the dotted lines. Increasing φ above φ_c, the long-time limits increase, as shown for $\phi_q^Z(t)$ for $q=7.4$ and $\zeta=0.80$. Decreasing φ below φ_c, the correlators cross the plateau at some time τ_β, and then decay towards zero. The decay from the plateau f_q^{xc} to zero is the α process for $\phi_q^x(t)$. It is characterized by a time scale τ_α, which can be defined, e.g., by $\phi_q^x(\tau_\alpha)=f_q^{xc}/2$. Upon decreasing $\varphi_c-\varphi$ towards zero, the time scales τ_β and τ_α increase towards infinity in proportion to t_σ and t'_σ, respectively, cited in Eq. (36). The figure exemplifies the standard MCT-bifurcation scenario. For small $|\varphi-\varphi_c|$, the results can be described in terms of scaling laws. This was explained in Refs. [22,23] for the HSS, and the discussion shall not be repeated here.

One can deduce from Fig. 2 that for $\zeta=0.80$ and $q\geqslant 5$ the plateaus for both types of density fluctuations are very close to each other: $f_q^{Nc}\approx f_q^{Zc}$. The upper two panels of Fig. 5 demonstrate that the dynamics as well is nearly the same, $\phi_q^N(t)\approx\phi_q^Z(t)$. This means that for $q\zeta>4$ and for strong steric hindrance, the cross correlations $F_q^{AB}(t)$ are very small. The reason is that the intramolecular correlation factors $j_\ell(q\zeta/2)$ are small, and thus interference effects between the density fluctuations of the two interaction sites are suppressed. Coherence effects can be expected only for smaller wave vectors. For this case, the functions can be understood in terms of their small-q asymptotes, Eq. (7).

The lower two panels in Fig. 5 deal with weak steric hindrance. In this case, the charge-density fluctuations behave quite differently from the number-density fluctuations. The most important origin of this difference is the reduction of the mode-coupling vertices $V_{q,kp}^Z$ relative to $V_{q,kp}^N$ in Eq. (22b). For small elongations of the molecule, the effective solute-solvent potentials for reorientations are small. Therefore, the f_q^{Zc} decrease strongly relative to f_q^{Nc} for ζ decreasing towards ζ_c, as is shown in Fig. 4. Upon approaching ζ_c, the α-peak strength of $\phi_q^Z(t)$ gets suppressed relative to that of $\phi_q^N(t)$. Within phase II, the charge-density fluctuations relax to zero as in a normal liquid. This implies as a precursor phenomenon that the time scale τ_α^Z of the charge-density-fluctuation α process decreases relative to the scale τ_α^N for the number-density fluctuations. Thus, the small-ζ behavior shown in the lower two panels of Fig. 5 is due to disturbances of the standard MCT-transition scenario by the nearby type-A transition.

The correlators $C_1(t)$ and $C_2(t)$ are shown in Fig. 6 for the critical point $\varphi=\varphi_c$ and for two liquid states near the transition from phase I to phase III. For $\zeta=0.80$, the anisotropic distribution of the solvent particles around the molecule leads to a stronger coupling to the dipole reorientations than to the reorientations for the quadrupole, and therefore the plateau for the former is higher than for the latter, $f_1^c>f_2^c$. A leading order expansion of the solutions of the equations of motion (28) and (32) in terms of the small parameter $C_\ell(t)-f_\ell^c$ leads to the factorization in the critical amplitude h_ℓ and a function $G(t)$ called the β correlator, $C_\ell(t)-f_\ell^c=h_\ell G(t)$. The latter is the same for all correlation functions. It obeys the first scaling law of MCT, $G(t)=\sqrt{|\sigma|}g_\pm(t/t_\sigma)$ for $\sigma\gtrless 0$. The master functions $g_\pm(\hat{t})$ are determined by λ.

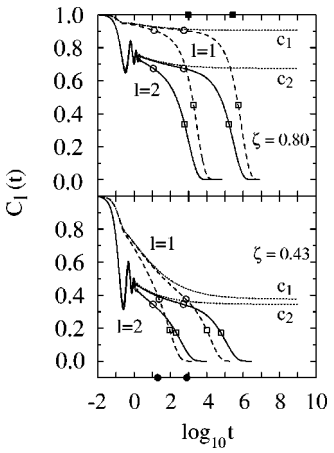

FIG. 6. Reorientational correlators $C_\ell(t)$ for $\ell=1$ (dashed lines) and $\ell=2$ (full lines) for two elongations ζ. The correlators for the critical packing fraction $\varphi=\varphi_c$ are shown as dotted lines marked with c_ℓ. The distance parameters $\epsilon=(\varphi-\varphi_c)/\varphi_c$ are -0.01 (faster decay) and -0.001 (slower decay). The full circles and squares mark the corresponding time scales t_σ and t'_σ, respectively, from Eq. (36). The open circles and squares on the curves mark the characteristic time scales τ^ℓ_β and τ^ℓ_α, respectively, defined by $C_\ell(\tau^\ell_\beta)=f^c_\ell$ and $C_\ell(\tau^\ell_\alpha)=f^c_\ell/2$.

They also describe the dynamics of the solvent in the window where $|\phi_q(t)-f^c_q|\ll 1$ [22]. In particular, there holds $g_-(\hat{t}_-)=0,\hat{t}_-=0.704$, so that both correlators $C_\ell(t)$ cross their plateau at the same time $\tau_\beta=\hat{t}_- t_\sigma$. The nonlinear mode-coupling effects require, that the correlators approach zero roughly at the same time. Thus one understands the general differences between the α processes, which were mentioned in the introduction: the α process for dipole relaxation is stronger, slower, and less stretched than those for quadrupole relaxation. This finding is in qualitative agreement with the ones of the theory based on tensor-density representation of the structure [14]. There are, however, quantitative differences between the two approximation schemes. The plateaus $f^c_1=0.905$ and $f^c_2=0.674$ are smaller than the corresponding values 0.943 and 0.835 found in Ref. [14] and the amplitudes $h_1=0.19$ and $h_2=0.40$ are bigger than the corresponding values 0.13 and 0.35 calculated previously [14]. The times τ^ℓ_α characterizing the α process shall be defined by $C_\ell(\tau^\ell_\alpha)=f^c_\ell/2$. They are marked by open squares in Fig. 6. The values $\tau^1_\alpha=5.21\times 10^5$, $\tau^2_\alpha=1.64\times 10^5$ for $x=3$ and $\zeta=0.80$ are smaller than those reported in Ref. [14]. The present theory implies a somewhat weaker coupling of the reorientational degrees of freedom of the molecule to the dynamics of the solvent than found earlier [14]. This holds also for the small elongation $\zeta=0.43$. The approach toward the transition from phase III to phase II leads to a suppression of f^c_1, as discussed for the f^{Zc}_q in Fig. 4. The dipole relaxation speeds up for $\zeta\to\zeta_c$, as discussed for the lower panels of Fig. 5. This is reflected by an enhancement of $h_1=1.60$ relative to the amplitudes cited for $\zeta=0.80$ but also relative to $h_2=0.49$.

One can perform $\lim_{\sigma\to 0-}\phi_q(\tilde{t}t'_\sigma)=\tilde{\phi}_q(\tilde{t})$ for the solutions of Eq. (14), where $\tilde{\phi}_q(\tilde{t})$ can be evaluated from the mode-coupling functional at the critical point. It obeys the initial condition $\tilde{\phi}_q(\tilde{t})=f^c_q-h_q\tilde{t}^b+O(\tilde{t}^{2b})$. Function $\tilde{\phi}_q(\tilde{t})$ can be considered as a shape function of the α process, and the result implies the second scaling law of MCT, also referred to as the superposition principle: $\phi_q(t)=\tilde{\phi}_q(t/t'_\sigma)$ for $\sigma\to 0-$ [26]. Corresponding laws hold for all functions, as is demonstrated in detail for the HSS in Refs. [22,23]. In particular, one gets for the reorientational correlators for $\sigma\to 0-$

$$C_\ell(t)=\tilde{C}_\ell(\tilde{t}),\quad \tilde{t}=t/t'_\sigma,\quad t_\sigma\ll t, \tag{38a}$$

and this corresponds to the α-scaling law for the susceptibility spectra

$$\chi''_\ell(\omega)=\tilde{\chi}''_\ell(\tilde{\omega}),\quad \tilde{\omega}=\omega t'_\sigma,\quad \omega\ll 1/t_\sigma. \tag{38b}$$

The initial decay of the master function $\tilde{C}_\ell(\tilde{t})$ is described by von Schweidler's law,

$$\tilde{C}_\ell(\tilde{t})=f^c_\ell-h_\ell\tilde{t}^b,\quad \tilde{t}\to 0, \tag{39a}$$

which is equivalent to a power-law tail of the master spectrum $\tilde{\chi}''_\ell(\tilde{\omega})$:

$$\tilde{\chi}''_\ell(\tilde{\omega})=h_\ell\sin(\pi b/2)\Gamma(1+b)/\tilde{\omega}^b,\quad \tilde{\omega}\to\infty. \tag{39b}$$

The upper panel of Fig. 7 exhibits the α-process master spectra for the reorientational processes for $\zeta=0.80$ and for the dimensionless longitudinal elastic modulus $m_{q=0}(t)$ of the solvent. The latter can be measured by Brillouin-scattering spectroscopy. It probes a tensor-density fluctuation for $\ell=0$. The von Schweidler law tails describe the spectra for frequencies exceeding the position $\tilde{\omega}_{\max}$ of the susceptibility maximum by a factor of about 100, as shown by the dashed lines. Since $f^c_1>f^c_2$ and both plateau values are rather large, one understands from the theory for the leading corrections to Eq. (39b) [22] that for decreasing $\tilde{\omega}$ the von Schweidler asymptote underestimates the spectrum, and does this by larger values for $\ell=1$ than for $\ell=2$. For smaller plateau values, the von Schweidler asymptote may overestimate the spectrum, as is exemplified for the modulus. The lower panel of Fig. 7 demonstrates that the α processes speed up if steric hindrance is decreased. As precursor of the transition to phase II, the spectrum for the dipole response is located at much higher frequencies than that for the quadrupole response. Traditionally, dielectric-loss spectra have been fitted by those of the Kohlrausch law $\phi_K(\tilde{t})=A\exp[-(\tilde{t}B)^\beta]$. Such fits also describe a major part of the spectra in Fig. 7, as shown by the dotted lines. The parameters A and B are adjusted to match the susceptibility maximum. The stretching exponent β is chosen so that the spectrum is fitted at half maximum $\tilde{\chi}''_\ell(\tilde{\omega}_{\max})/2$. If one denotes the width in $\log_{10}\omega$ at half maximum by W, stretching means that this parameter is larger than the value $W_D=1.14$ characterizing a Debye process, $\phi_D(\tilde{t})=\exp(-\tilde{t})$. The upper panel of Fig. 7 quantifies the general results of the theory for strong steric hindrance:

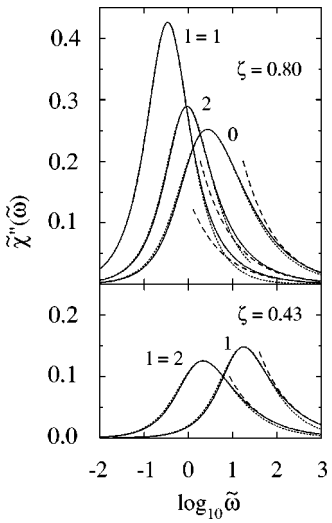

FIG. 7. Susceptibility master spectra $\tilde{\chi}''(\tilde{\omega})$ of the α process as a function of the logarithm of the rescaled frequency $\tilde{\omega}=\omega t'_\sigma$ (see text). Upper panel: curves $\ell=1$ and 2 refer to the response for the dipole and quadrupole, respectively, for elongation $\zeta=0.80$. Curve $\ell=0$ refers to the susceptibility master spectrum of the dimensionless longitudinal elastic modulus $m_{q=0}(t)$ of the HSS. The dashed lines exhibit the von Schweidler tails, Eq. (39b). The dotted lines are fits by Kohlrausch spectra $\tilde{\chi}''_K(\tilde{\omega})$ with stretching exponents $\beta=0.97$, 0.88, and 0.63 chosen for $\ell=1$, 2, and 0, respectively, so that the maximum and the full width at the half maximum W in decades of $\tilde{\chi}''_K(\tilde{\omega})$ agree with those of $\tilde{\chi}''(\tilde{\omega})$. The position of the susceptibility maximum is $\tilde{\omega}_{\max}=0.337$ (0.927, 2.69) and the width is $W=1.17$ (1.28, 1.76) for $\ell=1$ (2, 0). Lower panel: corresponding results for $\zeta=0.43$. The stretching exponent β, the maximum position $\tilde{\omega}_{\max}$, and the width W for $\ell=1$ ($\ell=2$) are $\beta=0.79$ (0.71), $\tilde{\omega}_{\max}=17.5$ (2.11), and $W=1.42$ (1.57), respectively.

$\tilde{\chi}''_1(\tilde{\omega}^1_{\max})>\tilde{\chi}''_2(\tilde{\omega}^2_{\max})$, $\tilde{\omega}^1_{\max}<\tilde{\omega}^2_{\max}$ and $\beta_1>\beta_2$. It quantifies also the fourth property cited in the Introduction, $\tilde{\omega}^2_{\max}<\tilde{\omega}^0_{\max}$. A further general property is $\beta_2>\beta_0$.

The discussion of power-law spectra is done more conveniently in a double logarithmic diagram as shown in Fig. 8 for normalized dipole-fluctuation-α-process spectra $\tilde{C}''_1(\tilde{\omega})\tilde{\omega}_{\max}/f_1^c=\tilde{\chi}''_1(\tilde{\omega})\tilde{\omega}_{\max}/f_1^c\tilde{\omega}$ as a function of $\tilde{\omega}/\tilde{\omega}_{\max}$. One notices that there is a white-noise spectrum for $\tilde{\omega}$ below $\tilde{\omega}_{\max}$. The high-frequency wing of the Kohlrausch-law fit decreases in proportion to $\tilde{\omega}^{-\beta}$ and underestimates the spectrum $\tilde{\chi}''_1(\tilde{\omega})$ considerably. Because of the von Schweidler asymptote, which is shown as a dashed straight line, the spectrum exhibits an enhanced high-frequency wing. Dixon *et al.* [31] made the remarkable observation that their dielectric spectra could be collapsed onto one master curve if the vertical axis is rescaled by w^{-1} and the horizontal axis by $w^{-1}(1+w^{-1})$, where $w=W/W_D$. In Fig. 8 this scaling is used and the data for glycerol from Ref. [31] are included. The spectra for molecules with $\zeta=0.80$ and $\zeta=0.60$, which are relevant for the description of van der Waals systems [14], follow the above-mentioned scaling surprisingly well. This finding appears nontrivial, since the scaling is not reproduced by the MCT results of the basic quantities $\phi_q(t)$ [32]. The rescaled spectrum for $\zeta=0.43$ deviates from the scaling law for $w^{-1}(1+w^{-1})\log_{10}(\tilde{\omega}/\tilde{\omega}_{max})\geqslant 5$.

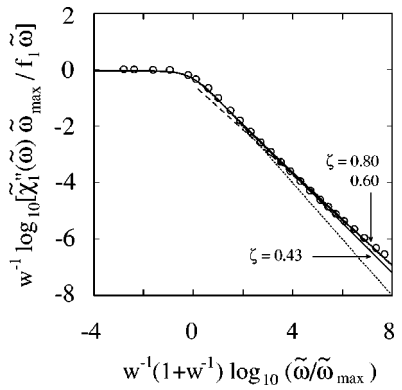

FIG. 8. Double logarithmic presentation of the normalized fluctuation spectra of the dipole-reorientation α processes, $\tilde{\chi}''_1(\tilde{\omega})\tilde{\omega}_{\max}/f_1^c\tilde{\omega}$, as a function of $\tilde{\omega}/\tilde{\omega}_{\max}$. Here $\tilde{\omega}_{\max}$ denotes the position of the susceptibility maximum. Following Dixon *et al.* [31], the vertical axis is rescaled by w^{-1} and the horizontal one by $w^{-1}(1+w^{-1})$, where $w=W/W_D$ is the ratio of the logarithmic full width at half maximum W of the susceptibility peak to the same quantity W_D of a Debye-peak. The open circles reproduce some of the dielectric-loss results for glycerol [31]. The three full lines from the top are the results for $\zeta=0.80$, 0.60, and 0.43, successively, although the upper two curves cannot be distinguished within the resolution of the figure. The dotted and the dashed lines exhibit the Kohlrausch fit with the stretching exponent $\beta=0.97$ and the von Schweidler law tail, respectively, for the $\zeta=0.80$ spectrum.

It might appear problematic that the dipole correlator was calculated within a different approximation scheme than the quadrupole correlator. But it is not difficult to also evaluate $C_1(t)$ within the scheme explained in Sec. III D for the evaluation of $C_2(t)$. Figure 9 presents a comparison of $C_1(t)$ obtained along the two specified routes. The two results for the small elongation $\zeta=0.43$ are close to each other. The discrepancies are mainly due to the 7% difference between

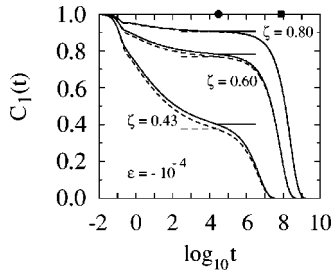

FIG. 9. Dipole correlators $C_1(t)$ for the distance parameter $\epsilon=-10^{-4}$ for three elongations ζ. The full circle and square indicate the times t_σ and t'_σ, respectively, from Eq. (36). The dashed lines are calculated from Eqs. (28) and (29). The plateaus $f_1^c=0.905$ (0.769, 0.376) for $\zeta=0.80$ (0.60, 0.43) are shown by dashed horizontal lines. The full lines exhibit $C_1(t)$ for the same states, but evaluated from equations derived in analogy to Eqs. (32)–(35), and their plateaus $f_1^c=0.907$ (0.782, 0.402) are indicated by full horizontal lines.

the two plateau values f_1^c. With increasing ζ, the discrepancies decrease. For the large elongation $\zeta=0.80$, the results are practically indistinguishable.

C. Structural relaxation versus transient dynamics

Let us introduce Fourier-Laplace transforms of functions of time, say, $f(t)$. There functions of frequency, say $f(\omega)$, are defined with the convention $f(\omega)=i\int_0^\infty dt\,\exp(izt)f(t)$, $z=\omega+i0$. The equations of motion (17) with the initial conditions from Eq. (5) are transformed into

$$[\omega\mathbf{1}+\mathbf{\Omega}_q^2\mathbf{m}_q(\omega)][\omega\mathbf{F}_q(\omega)+\mathbf{w}_q]-\mathbf{\Omega}_q^2\mathbf{F}_q(\omega)=\mathbf{0}. \quad (40)$$

Within the glass, the long-time limits of $\mathbf{F}_q(t)$ and $\mathbf{m}_q(t)$ do not vanish, i.e., the transformed quantities exhibit zero-frequency poles. One gets, for example, $\omega\mathbf{F}_q(\omega)\to-\mathbf{F}_q^\infty$ for $\omega\to0$, where the strength $-\mathbf{F}_q^\infty$ of the poles follows from Eq. (19). Continuity of the solutions of the MCT equation of motion implies that for vanishing frequencies and for vanishing distances from the transition points, $\mathbf{m}_q(\omega)$ becomes arbitrarily large. Hence, combinations like $\omega+i\xi_q$ with constants ξ_q can be neglected compared to $\mathbf{m}_q(\omega)$. Therefore, in the region of glassy dynamics, Eq. (40) can be modified to

$$\mathbf{F}_q(\omega)-\mathbf{m}_q(\omega)\mathbf{w}_q=i\boldsymbol{\xi}_q+\omega\mathbf{m}_q(\omega)\mathbf{F}_q(\omega). \quad (41)$$

Let us assume that this equation has a solution, to be denoted by $\mathbf{F}_q^*(\omega)$, which is defined for all frequencies, so that it can be back-transformed to a function $\mathbf{F}_q^*(t)$, defined for all $t>0$. Choosing $\boldsymbol{\xi}_q$ properly, Eq. (41) can be written as

$$\mathbf{F}_q^*(t)-\mathbf{m}_q^*(t)\mathbf{w}_q=-(d/dt)\int_0^t dt'\,\mathbf{m}_q^*(t-t')\mathbf{F}_q^*(t'). \quad (42a)$$

Similar reasoning leads from Eq. (14) to

$$\phi_q^*(t)-m_q^*(t)=-(d/dt)\int_0^t dt'\,m_q^*(t-t')\phi_q^*(t'). \quad (42b)$$

These formulas have to be supplemented with the MCT expressions for the kernels

$$\mathbf{m}_q^*(t)=\boldsymbol{\mathcal{F}}_q[\mathbf{F}^*(t),\phi^*(t)],\quad m_q^*(t)=\mathcal{F}_q[\phi^*(t)]. \quad (42c)$$

Equations (42) for the glassy dynamics are scale invariant. With one set of solutions $\phi_q^*(t)$ and $\mathbf{F}_q^*(t)$, the set $\phi_q^{*u}(t)=\phi_q^*(ut)$ and $\mathbf{F}_q^{*u}(t)=\mathbf{F}_q^*(ut)$ also provides a solution for arbitrary $u>0$. To fix the solution uniquely, one can introduce positive numbers y_q and positive definite matrices $\mathbf{y}_q$ to specify the initial condition as power-law asymptotes [16]:

$$\mathbf{F}_q^*(t)(t/t_0)^{1/3}\to\mathbf{y}_q,\quad \phi_q^*(t)(t/t_0)^{1/3}\to y_q,\quad (t/t_0)\to0. \quad (43)$$

The theory of the asymptotic solution of the MCT equations for simple systems had been built on the analogue of Eq. (41) with ξ_q neglected [22]. The present theory extends the previous one with the introduction of matrices. It seems obvious that the previous results for asymptotic expansions hold in a properly extended version. Let us only note the formula for the long-time decay of the correlators at the critical point $\varphi=\varphi_c$ [22,23]:

$$\mathbf{F}_q(t)=\mathbf{F}_q^{\infty c}+\mathbf{H}_q(t_0/t)^a\{\mathbf{1}+\mathbf{K}_q(t_0/t)^a+\mathbf{O}[(t_0/t)^{2a}]\}. \quad (44)$$

The exponent a, mentioned above, can be calculated from the mode-coupling functional at the critical point. The same is true for the plateau values $\mathbf{F}_q^{\infty c}$, and the amplitudes $\mathbf{H}_q$ and $\mathbf{K}_q$. The dependence of the solution from the transient dynamics is given by the single number t_0. Let us anticipate that Eq. (44) and similar results can be extended to a complete solution. One concludes that the glassy dynamics is determined, up to a scale t_0, by the mode-coupling functionals in Eq. (42c).

Equations (B11) and (B17) show that the mode-coupling functionals $\mathcal{F}_q$ and $\mathcal{F}_q^{ab}$ are specified by the density ρ, the static structure factor S_q, the direct correlation function c_q of the solvent, and the solute-solvent direct correlation functions c_q^a, i.e., by equilibrium quantities. They are the same for systems with a Newtonian dynamics, as considered in this paper, and for a model with a Brownian dynamics, as is to be used for the description of colloidal suspensions. In particular, the mode-coupling functionals are independent of the particle masses m, m_A, and m_B. Thus, the glassy dynamics of the molecule in the simple liquid does not depend on the inertia parameters specifying the microscopic equations of motion. The same conclusions on the glassy dynamics, which were cited in the Introduction for the basic version of MCT, hold for the model studied in this paper. Let us add that neither the temperature T nor the interparticle-interaction potentials V of the solvent, nor the solute-solvent-interaction potentials V^a, enter explicitly into the mode-coupling functionals. These quantities only enter implicitly via S_q, c_q, c_q^A, and c_q^B.

The independence of the glassy dynamics from the inertia parameters is demonstrated in Fig. 10 for four states of the liquid. It is shown that the reorientational dynamics of the dipole does not change for $t>1$ even if the mass ratio of the atoms m_A/m_B is altered by a factor of 10. The transient dynamics, which deals with overdamped librations, exhibits an isotope effect. There is no fitting parameter involved in the diagram shown. The scale t_0 depends neither on the density of the solvent nor on the elongation parameter, and Eqs. (42) describe the complete control-parameter dependence of the glassy dynamics.

V. SUMMARY

The MCT for simple systems with a dilute solute of atoms has been generalized to one with a dilute solute of diatomic molecules. The derived equations of motion generalize the ones for atoms in the sense that scalar functions are replaced by 2×2 matrix functions. These generalizations result from the description of the position of the molecule in terms of interaction-site-density fluctuations. The numerical effort re-

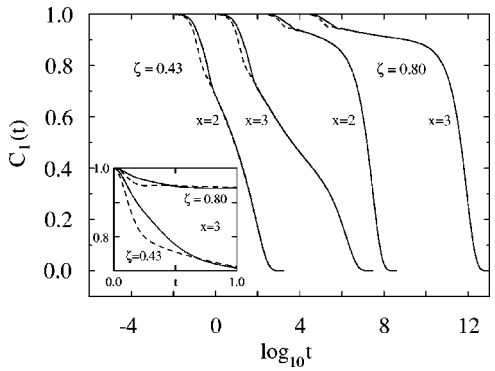

FIG. 10. Dipole correlators $C_1(t)$ for a dumbbell of two fused hard spheres of diameters d and distance ζd between the centers moving in a liquid of hard spheres with diameter d for a distance parameter $(\varphi-\varphi_c)/\varphi_c=-10^{-x}$. The dashed lines reproduce the results from Fig. 6 and refer to a symmetric molecule with masses of the two atoms being equal to the mass m of the solvent particles $m_A=m_B=m$. The full lines exhibit the results for an asymmetric dumbbell with $m_A=10m$, $m_B=m$. In the main frame the results for different states are successively shifted horizontally by a factor 100 in order to avoid overcrowding. The inset shows the transient dynamics on a linear time axis.

quired for a solution of the equations is not substantially larger than the one needed to solve the corresponding equations for atomic solutes. This holds in particular for symmetric molecules where the matrix equations can be diagonalized by a linear transformation to number-density and charge-density fluctuations. The theory implies that the dynamics outside the transient regime is determined, up to an overall time scale t_0, by the equilibrium structure. In particular, it is independent of the inertia parameters of the system.

It was shown that the present theory reproduces all qualitative results obtained within the preceding much more involved theory based on a description of the solute by tensor-density fluctuations. Both theories yield a similar phase diagram, Fig. 1. The characteristic differences of the reorientational correlators exhibited for strong steric hindrance of rotations as opposed to weak steric hindrance are obtained here, in Fig. 6, as previously. There are systematic quantitative differences between the two approximation approaches in the sense that the implications of the cage effect are weaker in the present theory than in the preceding work [13,14]. The earlier findings on the differences between the spectra for the responses with angular-momentum index $\ell=0$, 1, and 2 have been corroborated by separating the α peaks from the complete spectra with the aid of the α-scaling law, Fig. 7.

The critical nonergodicity parameters f_q^{xc} have been calculated; these determine the form factors of quasielastic scattering from the liquid near the glass transition. Contrary to what one finds for atomic solutes, these are not bell-shaped functions of wave numbers q; rather they exhibit kinks; see Fig. 2. The form factors for some wave numbers q vary nonmonotonically with changes of the elongation of the molecule, Fig. 4. Analyzing these findings in terms of form factors defined for fixed angular-momentum index ℓ, one can explain the results as being due to intramolecular interference effects demonstrating that the theory accounts for reorientational correlations with angular-momentum index $\ell \geqslant 2$.

It was shown that the α-relaxation spectra for dipole reorientations with strong steric hindrance obey the scaling law proposed by Dixon *et al.* [31] within the window and within the accuracy level considered by these authors. There is no fitting parameter involved in the construction of Fig. 8, which demonstrates this finding for the two elongation parameters $\zeta=0.60$ and 0.80. Thus, it is not justified to use the cited empirical scaling as an argument against the applicability of MCT for a discussion of dielectric-loss spectra.

ACKNOWLEDGMENTS

We thank M. Fuchs, M. Sperl, and Th. Voigtmann for many helpful discussions and suggestions. We are grateful to A. Latz and R. Schilling for constructive critiques of our manuscript. S.-H.C. acknowledges financial support from Japan Society for the Promotion of Science for Research Abroad. This work was supported by Verbundprojekt BMBF 03-G05TUM.

APPENDIX A: TENSOR-DENSITY REPRESENTATIONS

Following the conventions of Refs. [13] and [14], normalized tensor-density fluctuations shall be used by decomposing the molecule's position variable in plane waves $\exp(i\vec{q}\cdot\vec{r}_C)$ for the center of mass $\vec{r}_C$ and in spherical harmonics $Y_\ell^m(\vec{e})$ for the orientation vector $\vec{e}$:

$$\rho_\ell^m(\vec{q})=i^\ell\sqrt{4\pi}\exp(i\vec{q}\cdot\vec{r}_C)Y_\ell^m(\vec{e}). \tag{A1}$$

The molecule-solvent interactions are specified by a set of direct correlation functions

$$c_\ell(q)=\langle\rho_{\vec{q}_0}^{*}\rho_\ell^0(\vec{q}_0)\rangle/(\rho S_q);\quad \vec{q}_0=(0,0,q). \tag{A2}$$

The structure dynamics is described by the matrix of correlators, defined by

$$\phi_{\ell k}(qm,t)=\langle\rho_\ell^m(\vec{q}_0,t)^*\rho_k^m(\vec{q}_0)\rangle. \tag{A3}$$

Since the position vectors of the interaction sites can be written as $\vec{r}_a=\vec{r}_C+z_a\vec{e}$, the Rayleigh expansion of the exponential in Eq. (1) yields the formula

$$\rho_{q_0}^a=\sum_\ell\sqrt{2\ell+1}j_\ell(qz_a)\rho_\ell^0(\vec{q}_0). \tag{A4}$$

Substitution of this expression into Eq. (3) leads, with Eq. (A2), to an expression connecting the direct correlation functions c_q^a with $c_\ell(q)$:

$$\sum_b w_q^{ab}c_q^b=\sum_\ell\sqrt{2\ell+1}j_\ell(qz_a)c_\ell(q). \tag{A5}$$

Substitution of Eq. (A4) into Eq. (4) leads, with Eq. (A3), to the expression of the site-density correlators in terms of the tensor-density correlators:

$$F_q^{ab}(t)=\sum_{\ell k}\sqrt{(2\ell+1)(2k+1)}j_\ell(qz_a)j_k(qz_b)\phi_{\ell k}(q0,t). \tag{A6}$$

For the long-time limits of the correlators $F_q^{ab}(t)$ one gets a combination of the nonergodicity parameters $f_{\ell k}(qm)=\phi_{\ell k}(qm,t\to\infty)$. If one uses the diagonal approximation $f_{\ell k}(q,m)=\delta_{\ell k}f(q\ell m)$, one can write

$$F_q^{ab}(t\to\infty)=\sum_{\ell}(2\ell+1)j_\ell(qz_a)j_\ell(qz_b)f(q\ell 0). \tag{A7}$$

Substituting the Rayleigh expansion of Eq. (1) into Eq. (34a), one can express the pair modes in terms of those formed with tensor-density fluctuations:

$$A^a(\vec{k},\vec{p})=\sqrt{4\pi}\sum_{\ell m}j_\ell(kz_a)Y_\ell^m(\vec{k})[\rho_\ell^m(\vec{k})\rho_{\vec{p}}/\sqrt{NS_p}]. \tag{A8}$$

Therefore, the overlaps of the forces with the pair modes can be expressed as sums of the corresponding quantities calculated in Ref. [13]. One finds for the mode-coupling coefficients in Eq. (35)

$$V_2^{ab}(k)=[k^2\rho S_k/2\pi^2]\sum_{cd}(\mathbf{w}_k^{-1})^{ac}D_c(k)D_d(k)(\mathbf{w}_k^{-1})^{db}. \tag{A9a}$$

Here one gets for $a=A$, B, or C

$$D_a(k)=\frac{1}{12}\sum_{\ell J}(-1)^{1/2(\ell+J)}(2\ell+1)\sqrt{2J+1}j_\ell(kz_a)c_J(k)\times[J(J+1)+6-\ell(\ell+1)]\begin{pmatrix}2&\ell&J\\0&0&0\end{pmatrix}^2, \tag{A9b}$$

where the last factor denotes Wigner's 3-j symbol.

APPENDIX B: MODE-COUPLING COEFFICIENTS

Mode-coupling equations based on a description of the molecules by site-density fluctuations have been derived in Ref. [18] by extending the procedure used originally for atomic systems [26]. But the reported formulas [18] do not seem appropriate, since they do not reduce to the ones for tagged particle motion if the limit of a vanishing elongation parameter ζ is considered. Therefore, an alternative derivation will be presented which starts from the theory developed by Mori and Fujisaka [33] for an approximate treatment of nonlinear fluctuations. The application of this theory will be explained by rederiving the equations for the solvent before the ones for the solute are worked out.

1. The Mori-Fujisaka equations

Let us consider a set of distinguished dynamical variables $A_\alpha,\alpha=1,2,\ldots,$ defined as functions on the system's phase space. The time evolution is generated by the Liouvillian $A_\alpha(t)=\exp(i\mathcal{L}t)A_\alpha$. Using canonical averaging to define scalar products in the space of variables, $(A,B)=\langle A^*B\rangle$, the Liouvillian is Hermitian. The goal is to derive equations of motion for the matrix of correlators $C_{\alpha\beta}(t)=(A_\alpha(t),A_\beta)$. The initial condition is given by the positive definite matrix $g_{\alpha\beta}=(A_\alpha,A_\beta)$. The theory starts with a generalized Fokker-Planck equation for the distribution function $g_a=\Pi_\alpha\delta(A_\alpha-a_\alpha)$, $a=(a_1,a_2,\ldots)$. It is assumed that the time scales for the fluctuations of the A_α and their products are larger than those for the Langevin fluctuating forces. The spectra of the latter can then be approximated by a constant matrix $\Gamma_{\alpha\beta}$. It is assumed, furthermore, that the $\Gamma_{\alpha\beta}$ are independent of the distinguished variables, and that the equilibrium distribution of the latter is Gaussian:

$$\langle g_a\rangle=C\exp\left(-\frac{1}{2}\sum_{\alpha\beta}a_\alpha g_{\alpha\beta}^{-1}a_\beta^*\right). \tag{B1}$$

In the cited Fokker-Planck equation there occurs the streaming velocity $v_\alpha(a)$ given by

$$v_\alpha(a)\langle g_a\rangle=\langle\dot{A}_\alpha^*g_a\rangle=k_BT\sum_\beta\frac{\partial}{\partial a_\beta}\langle\{A_\alpha^*,A_\beta\}g_a\rangle. \tag{B2}$$

The Fokker-Planck equation is now reduced by projecting out the subspace of the distinguished variables. There appears the frequency matrix specifying the linear contribution to the streaming term,

$$\Omega_{\alpha\beta}=\sum_\gamma(A_\alpha,\mathcal{L}A_\gamma)g_{\gamma\beta}^{-1}. \tag{B3}$$

The nonlinear contributions enter as combination

$$f_\alpha=\int da\,v_\alpha(a)g_a-i\sum_\beta\Omega_{\alpha\beta}A_\beta. \tag{B4}$$

They determine the relaxation kernel as

$$M_{\alpha\beta}(t)=\sum_\gamma(f_\alpha(t),f_\gamma)g_{\gamma\beta}^{-1}. \tag{B5}$$

The time evolution is generated by the reduced Liouvillian $\mathcal{L}'=\mathcal{Q}L\mathcal{Q}$, $f_\alpha(t)=\exp(i\mathcal{L}'t)f_\alpha$, where $\mathcal{Q}$ is the projector on the space perpendicular to the one spanned by the distinguished variables. The result, which is equivalent to Eq. (2.15) in Ref. [33], reads

$$\partial_tC_{\alpha\beta}(t)=-\sum_\gamma\left[(i\Omega_{\alpha\gamma}+\Gamma_{\alpha\gamma})C_{\gamma\beta}(t)+\int_0^t dt'M_{\alpha\gamma}(t-t')C_{\gamma\beta}(t')\right]. \tag{B6}$$

2. MCT equations for simple systems

To get a description of slowly varying structural fluctuations, the original reasoning of MCT shall be adopted, and as

distinguished variables the density fluctuations $\rho_{\vec{q}}$ and the longitudinal current fluctuations $j_{\vec{q}}=\Sigma_\kappa v_{\kappa,z}\exp(i\vec{q}\cdot\vec{r}_\kappa)$ will be chosen. The variable label of the preceding subsection consists of two bits, $\alpha=(\lambda,\vec{q})$, $\lambda=1,2$, so that $A_{1\vec{q}}=\rho_{\vec{q}}$, $A_{2\vec{q}}=j_{\vec{q}}$. Notations are the same as those of the first paragraph of Sec. II. One gets $g_{1\vec{q}1\vec{q}}=NS_q$, $g_{2\vec{q}2\vec{q}}=Nv^2$, $\Omega_{1\vec{q}2\vec{q}}=q$, $\Omega_{2\vec{q}1\vec{q}}=\Omega_q^2/q$, and all the other elements of the matrices g and Ω are zero. Because of translational invariance, one gets $C_{\lambda\vec{q}\mu\vec{k}}(t)=0$ unless $\vec{q}=\vec{k}$, and rotational invariance implies that $C_{\lambda\vec{q}\mu\vec{q}}(t)$ depends on the modulus q only. The same holds for the matrices Γ and M, so that Eq. (B6) reduces to a 2×2 matrix equation with q appearing as a parameter. Since $\mathcal{L}\rho_{\vec{q}}$ is an element of the distinguished set of variables, the kernels $\Gamma_{\alpha\beta}$ and $M_{\alpha\beta}(t)$ vanish unless $\alpha=\beta=(2,\vec{q})$. The latter shall be denoted by Γ_q and $M_q(t)$, respectively. Equation (B6) can then be reduced to the equation of motion for the normalized density correlator $\phi_q(t)=C_{1\vec{q}1\vec{q}}(t)/NS_q$:

$$\partial_t^2\phi_q(t)+\Gamma_q\partial_t\phi_q(t)+\Omega_q^2\phi_q(t)+\int_0^t dt' M_q(t-t')\partial_{t'}\phi_q(t')=0. \tag{B7}$$

The application of the Mori-Fujisaka formalism can be summarized as follows. The relaxation kernel $\Omega_q^2 m_q(t)$ of the exact Eq. (14) is approximately split into a white noise contribution $2\Gamma_q\delta(t)$ and a remainder $M_q(t)$, where well defined formulas for the two contributions are available. In this paper, the kernel Γ_q is neglected and Eq. (B5) for the kernel,

$$M_q(t)=(f_{\vec{q}}(t),f_{\vec{q}})/Nv^2,\quad f_{\vec{q}}=f_{2\vec{q}}, \tag{B8}$$

shall be approximated further.

If one writes $a_{1\vec{q}}=\tilde{\rho}_{\vec{q}}$ and $a_{2\vec{q}}=\tilde{j}_{\vec{q}}$, one can denote the equilibrium distribution $w(a)=\langle g_a\rangle$ for the solvent variables as

$$w(a)=C\exp\left\{-(1/2N)\sum_{\vec{q}}\left[(1-\rho c_q)\tilde{\rho}_{\vec{q}}\tilde{\rho}_{\vec{q}}^{\,*}+(1/v^2)\tilde{j}_{\vec{q}}\tilde{j}_{\vec{q}}^{\,*}\right]\right\}. \tag{B9}$$

This is used to derive from Eqs. (B2) and (B4)

$$f_{\vec{q}}=-i(\rho v^2/N)\sum_{\vec{k}}(\vec{k}\cdot\vec{q}/q)c_k\rho_{\vec{k}}\rho_{\vec{q}-\vec{k}}+\delta f_{\vec{q}}, \tag{B10}$$

where $\delta f_{\vec{q}}$ denotes a term whose contribution to the memory kernel turns out to be irrelevant for the structural relaxation processes, and therefore shall be neglected. The remaining task is the evaluation of averages $(\rho_{\vec{k}}(t)\rho_{\vec{p}}(t),\rho_{\vec{k}'}\rho_{\vec{p}'})$, where the time evolution is generated by the reduced Liouvillian. Here the original MCT ansatz is used: $(\rho_{\vec{k}}(t)\rho_{\vec{k}'})(\rho_{\vec{p}}(t)\rho_{\vec{p}'})+(k\leftrightarrow p)$. As a result, one gets $M_q(t)=\Omega_q^2 m_q(t)$ with the well known expression for the mode-coupling functional in Eqs. (15):

$$\mathcal{F}_q[\tilde{f}]=(\rho/16\pi^3q^4)\int d\vec{k}S_qS_kS_p[\vec{q}\cdot\vec{k}c_k+\vec{q}\cdot\vec{p}c_p]^2\tilde{f}_k\tilde{f}_p, \tag{B11}$$

with $\vec{p}=\vec{q}-\vec{k}$.

3. MCT equations for the solute molecule

It is straightforward to generalize the preceding derivation to systems with a diatomic solute molecule provided the latter is considered flexible. Therefore, let us use this modification of the problem. It will be assumed that the kinetic energy of the molecule is $\Sigma_a(m_a/2)\vec{v}_a^2$ and that there is a binding potential $V^{f\!\!/}(|\vec{r}_A-\vec{r}_B|)$ between the two interaction sites. The exact Eq. (17a) remains valid with the frequency matrix replaced by that of the flexible molecule $\Omega_q^{f\!\!/2}$. It is defined via Eq. (17b) with the simple velocity correlator $J_q^{f\!\!/ab}=\delta^{ab}(k_BT/m_a)$.

The formulas of Sec. B 1 shall be applied with the extended set of densities $(\rho_{\vec{q}},\rho_{\vec{q}}^{\,A},\rho_{\vec{q}}^{\,B})$ and the corresponding longitudinal currents $(j_{\vec{q}},j_{\vec{q}}^{\,A},j_{\vec{q}}^{\,B})$. Thus the index consists of three bits $\alpha=(\tau,\lambda,\vec{q})$, where $\lambda=1,2$ discriminates between densities and currents, and $\tau=O,A,B$ indicates solvent, atom A, and atom B, respectively. In the infinite dilution limit $N\to\infty$, the equations for the solute do not directly couple to those for the solvent. Therefore, Eq. (B7) remains valid and one gets a modification of Eq. (17a) for the solute:

$$\partial_t^2\mathbf{F}_q(t)+\mathbf{\Gamma}_q\partial_t\mathbf{F}_q(t)+\mathbf{\Omega}_q^{f\!\!/2}\mathbf{F}_q(t)+\int_0^t dt'\mathbf{M}_q(t-t')\partial_{t'}\mathbf{F}_q(t')=\mathbf{0}. \tag{B12}$$

The relaxation kernel reads

$$M_q^{ab}(t)=(f_{\vec{q}}^{\,a}(t),f_{\vec{q}}^{\,b})(m_b/k_BT),\quad f_{\vec{q}}^{\,a}=f_{a2\vec{q}}. \tag{B13}$$

The determination of the Gaussian distribution of the extended distinguished variables requires the inversion of the 3×3 matrix $(A_{\tau1\vec{q}},A_{\sigma1\vec{q}})$. Making use of the infinite dilution limit $N\to\infty$, one gets

$$\langle g_a\rangle=w^O(a)\exp\left\{(1/2)\sum_{\vec{q}}\sum_{ab}\left[(2\rho/N)\delta^{ab}c_q^a\tilde{\rho}_{\vec{q}}\tilde{\rho}_{\vec{q}}^{\,a*}-(\mathbf{w}_q^{-1})^{ab}\tilde{\rho}_{\vec{q}}^{\,a}\tilde{\rho}_{\vec{q}}^{\,b*}-(m_a/k_BT)\delta^{ab}\tilde{j}_{\vec{q}}^{\,a}\tilde{j}_{\vec{q}}^{\,b*}\right]\right\}, \tag{B14}$$

where $w^O(a)$ is the distribution for the solvent variables given by Eq. (B9). This expression is used to work out the fluctuating force as explained in connection with Eq. (B10):

$$f_{\vec{q}}^{\,a}=-i(\rho/N)(k_BT/m_a)\sum_{\vec{k}}[(\vec{q}-\vec{k})\cdot\vec{q}/q]c_k^a\rho_{\vec{k}}^a\rho_{\vec{q}-\vec{k}}+\delta f_{\vec{q}}^{\,a}. \tag{B15}$$

As above, the contributions due to $\delta f_{\vec{q}}^{a}$ are neglected and the remaining pair correlations are factorized. This leads to

$$\mathbf{M}_q(t) = \mathbf{\Omega}_q^{f\prime 2}\mathbf{m}_q(t), \tag{B16}$$

where the functional for the kernel in Eq. (18a) reads

$$\mathcal{F}_q^{ab}[\tilde{\mathbf{f}},\tilde{f}] = q^{-2}\sum_c w_q^{ac}(\rho/8\pi^3)\int d\vec{k}(\vec{q}\cdot\vec{p}/q)^2 S_p c_p^c c_p^b \tilde{f}_k^{cb}\tilde{f}_p, \tag{B17}$$

with $\vec{p}$ abbreviating $\vec{q}-\vec{k}$. Neglecting the friction term $\mathbf{\Gamma}_q$ in Eq. (B12), the MCT equations (17) and (18) are derived for the flexible molecule.

Obviously, a theory for a rigid molecule can be obtained from one for a flexible molecule only within a quantum-mechanical approach. One has to consider the case where excitation energies for translational and rotational motion are small compared to the thermal energy, while the energies for vibrational excitations are large. Let us assume that the formulas can be obtained by replacing all equilibrium averages in the preceding equations with the correct quantum mechanical ones, where the latter can be evaluated for the classical molecule model with five degrees of freedom. This amounts to replacing structure functions with the classical quantities, in particular the replacement of $\mathbf{\Omega}_q^{f\prime}$ by $\mathbf{\Omega}_q$. Thereby Eq. (B12) produces Eqs. (17).

[1] W. van Megen, Transp. Theory Stat. Phys. **24**, 1017 (1995).
[2] M. Nauroth and W. Kob, Phys. Rev. E **55**, 657 (1997).
[3] T. Gleim, W. Kob, and K. Binder, Phys. Rev. Lett. **81**, 4404 (1998).
[4] T. Gleim and W. Kob, Eur. Phys. J. B **13**, 83 (2000).
[5] W. Götze and L. Sjögren, Rep. Prog. Phys. **55**, 241 (1992).
[6] W. Götze, J. Phys.: Condens. Matter **11**, A1 (1999).
[7] R. Schilling and T. Scheidsteger, Phys. Rev. E **56**, 2932 (1997).
[8] C. Theis and R. Schilling, J. Non-Cryst. Solids **235–237**, 106 (1998).
[9] L. Fabbian, A. Latz, R. Schilling, F. Sciortino, P. Tartaglia, and C. Theis, Phys. Rev. E **60**, 5768 (1999).
[10] A. Winkler, A. Latz, R. Schilling, and C. Theis, e-print cond-mat/0007276.
[11] C. Theis, F. Sciortino, A. Latz, R. Schilling, and P. Tartaglia, Phys. Rev. E **62**, 1856 (2000).
[12] M. Letz, R. Schilling, and A. Latz, Phys. Rev. E **62**, 5173 (2000).
[13] T. Franosch, M. Fuchs, W. Götze, M. R. Mayr, and A. P. Singh, Phys. Rev. E **56**, 5659 (1997).
[14] W. Götze, A. P. Singh, and Th. Voigtmann, Phys. Rev. E **61**, 6934 (2000).
[15] T. Franosch, W. Götze, M. R. Mayr, and A. P. Singh, J. Non-Cryst. Solids **235–237**, 71 (1998).
[16] M. Fuchs and Th. Voigtmann, Philos. Mag. B **79**, 1799 (1999).
[17] K. Kawasaki, Physica A **243**, 25 (1997).
[18] S.-H. Chong and F. Hirata, Phys. Rev. E **58**, 6188 (1998).
[19] D. Chandler and H. C. Andersen, J. Chem. Phys. **57**, 1930 (1972).
[20] J.-P. Hansen and I. R. McDonald, *Theory of Simple Liquids*, 2nd ed. (Academic Press, London, 1986).
[21] S.-H. Chong and F. Hirata, Phys. Rev. E **57**, 1691 (1998).
[22] T. Franosch, M. Fuchs, W. Götze, M. R. Mayr, and A. P. Singh, Phys. Rev. E **55**, 7153 (1997).
[23] M. Fuchs, W. Götze, and M. R. Mayr, Phys. Rev. E **58**, 3384 (1998).
[24] J. S. Høye and G. Stell, J. Chem. Phys. **66**, 795 (1977).
[25] D. E. Sullivan and C. G. Gray, Mol. Phys. **42**, 443 (1981).
[26] W. Götze, in *Liquids, Freezing and Glass Transition*, edited by J.-P. Hansen, D. Levesque, and J. Zinn-Justin (North-Holland, Amsterdam, 1991), p. 287.
[27] W. Götze and M. R. Mayr, Phys. Rev. E **61**, 587 (2000).
[28] T. Franosch and A. P. Singh, J. Chem. Phys. **107**, 5524 (1997).
[29] T. Franosch and A. P. Singh, J. Non-Cryst. Solids **235–237**, 153 (1998).
[30] T. Franosch and W. Götze, J. Phys.: Condens. Matter **6**, 4807 (1994).
[31] P. K. Dixon, L. Wu, S. R. Nagel, B. D. Williams, and J. P. Carini, Phys. Rev. Lett. **65**, 1108 (1990).
[32] M. Fuchs, I. Hofacker, and A. Latz, Phys. Rev. A **45**, 898 (1992).
[33] H. Mori and H. Fujisaka, Prog. Theor. Phys. **49**, 764 (1973).